# 14

# Quantum Mechanics of Semiconductor Quantum Dots and Rings

I. Filikhin, S.G. Matinyan and B. Vlahovic
*North Carolina Central University*
*USA*

## 1. Introduction

The progress of semiconductor physics in the decade 1970-1980 is connected with gradual deviation from the electronic band structure of ideal crystal of Bloch picture (Bloch, 1928) where, unlike atomic world with its discrete and precisely defined, in the limits of uncertainty relation, energy levels, energy of bound electron is a multivalued function of momentum in the energy band and density of states are continuous (For the earlier short but comprehensive survey see (Alferov, 1998)).

In principle, Bloch theory deals with infinite extension of lattice, with the understandable (and important) surface effects. The decreasing of the size of the object to a few micrometers principally does not change the picture of the extended crystal qualitatively. It takes a place until one reaches the scale where the size quantization essentially enters the game and we can speak about microscopic limit of matter. What generally divides macroscopic limit of the solid state from the microscopic one? It is defined by some correlation length (or, more generally, all such relevant lengths)): for carriers it is mean free path length $l$ or Broglie length $l_B = h/p$ ($p$-momentum), which is smaller. One may say that the quantum mechanical properties of matter clearly reveal if $l/a \geq 1$, where $a$ is the size of the lattice constant. In the opposite limit $l/a < 1$, matter is considered macroscopically.

In this light, it is worthy to remind that as long as 1962, L. V. Keldysh (Keldysh, 1962 as cited in Bimberg et al., 1999) considered electron motion in a crystal with periodic potential with the period that is much larger than the lattice constant. In this limit he discovered so called minizones and negative resistance. Just in this limit $l/a \geq 1$ we expect the size quantization with its discrete levels and coherence in the sense that electron can propagate across the whole system without scattering, its wave function maintains a definite phase. In this limit, mesoscopic (term coined by van Kampen (1981) relates to the intermediate scale dividing the macro and micro limits of matter) and nanoscopic objects (Quantum Wells (QW), Wires and Dots (QD)) shown very interesting quantum mechanical effects. In this limit many usual rules of macroscopic physics may not hold. For only one example, rules of addition of resistance both in series and parallel are quite different and more complicated (Landauer, 1970; Anderson et al., 1980; Gefen, et al., 1984).

Closing this brief introduction concerning some aspects of genuine quantum objects (QW, Q Wires, QD) we would like to emphasize the conditional sense of the notion of dimensions in

this world: in the limit $l/a \geq 1$ dimensions are defined as difference between real spatial dimension (in our world $D$ =3) and numbers of the confined directions: Quantum Well: $D$ =2, Quantum Wire: $D$ =1, Quantum Dot: $D$ =0. However, for example, QD which will be one of our subject for study, has very rich structure with many discrete levels, their structure define the presence or absence of Chaos, as we will see below, inside QD. Minimal size of QD is defined by the condition to have at least one energy level of electron (hole) or both: $a_{\min} = \pi\hbar / \sqrt{2m^* \Delta E} \approx 4$ nm, where $\Delta E$ is average distance between neighboring energy levels. Maximal size of QD is defined by the conditions that all three dimensions are still confined. It depends, of course, on temperature: at room temperature it is 12 nm (GaAs), 20 nm (InAs) ($\Delta E \approx 3kT$). The lower temperature, the wider QD is left as quantum object with $D$ =0 and the number of energy levels will be higher.

## 2. Effective model for semiconductor quantum dots

The effective potential method has been developed (Filikhin et al., 2006) to calculate the properties of realistic semiconductor quantum dot/ring (QD/QR) nanostructures with the explicit consideration of quantum dot size, shape, and material composition. The method is based on the single sub-band approach with the energy dependent electron effective mass. In this approach, the confined states of carriers are formed by the band gap offset potential. Additional effective potential is introduced to account for cumulative band gap deformations due to strain and piezoelectric effects inside the quantum dot nanostructure. The magnitude of the effective potential is selected in such a way as to reproduce experimental data for a given nanomaterial. Additionally, an analog of the Kane formula (Kane, 1957) is implemented in the model to take into account the non-parabolicity of the conduction/valence band. The resulting nonlinear eigenvalue problem for the Schrödinger equation is solved by means of the iterative procedure with the adjusted effective electron mass and non-parabolicity parameter, where in each iteration step the Schrödinger equation is numerically linearized and solved by the finite element method.

At present, simulations based on this approach are performed for the InGaAs/GaAs quantum dots and quantum rings of different sizes and configurations under different external conditions. The obtained results show that the residual strain and conduction band non-parabolicity effects greatly affect the device related properties of semiconductor quantum dots. The results are in good agreement with available experimental data, closely matching energy level and effective mass data extracted from capacitance–voltage experiments. The method also allows one to accurately simulate spin-orbital coupling effects for the electrons in excited states, as well as the presence of admixtures, such as Ga. Our calculations of the Coulomb shifts of the exciton complexes (positively and negatively charged trions, biexcitons) in the InGaAs/GaAs quantum dots with 22%-25% Ga fraction match very well both capacitance-voltage and photoluminescence measurements. To best reproduce the experimental data, Ga fraction in the InGaAs/GaAs quantum dots should not exceed 25%.

Commonly used numerical approaches, such as the 8-band ***kp***-theory, density functional theory, or atomistic pseudo-potential technique, take into account inter-band interactions, strain and piezoelectric effects in quantum dots in an *ab initio* manner. Such methods are very computationally intensive and time-consuming. The important advantage of the effective model is that the high accuracy of calculations is obtained at a very low

computational cost – calculations can typically be completed using a 3 GHz PC with 1 GB of memory in less than 20 minutes. The effective potential method satisfactorily reproduces the results of the realistic simulations, thus offering an independent evaluation of the electronic confinement effects calculated within others models.

### 2.1 Formalism

#### 2.1.1 Schrödinger equation and effective mass approximation

In the present review a semiconductor 3D heterostructure (QD or QR) is modeled utilizing a ***kp***-perturbation single sub-band approach with quasi-particle effective mass (Harrison, 2005; Manasreh, 2005; Yu & Cardona, 2005). The energies and wave functions of a single carrier in a semiconductor structure are solutions the Schrödinger equation:

$$(H_{kp} + V_c(\vec{r}))\Psi(\vec{r}) = E\Psi(\vec{r}) \tag{1}$$

Here $H_{kp}$ is the single band ***kp***-Hamiltonian operator, $H_{kp} = -\nabla\frac{\hbar^2}{2m^*(\vec{r})}\nabla$, $m^*$ is the electron/hole effective mass for the bulk, which may depend on coordinate, and $V_c(\vec{r})$ is the confinement potential. The confinement of the single carrier is formed by the energy misalignment of the conduction (valence) band edges of the QD material (index 1) and the substrate material (index 2) in the bulk. $V_c(\vec{r})$ is so called "band gap potential". The magnitude of the potential is proportional to the energy misalignment. The band structure of the single band approximation can be found in many textbooks (see, for example, (Harrison, 2005; Manasreh, 2005; Yu & Cadona, 2005). * (see the input below) $\Psi(\vec{r})$ and its derivative $1/m^*(\vec{n},\nabla)\Psi(\vec{r})$ on interface of QD and the substrate are continues.

#### 2.1.2 The non-parabolicity of the conduction band. The Kane formula

Traditionally applied in the macroscopic scale studies parabolic electron spectrum needs to be replaced by the non-parabolic approach, which is more appropriate to nano-sized quantum objects (Wetzel et al., 1996; Fu et al., 1998). The Kane formula (Kane, 1957) is implemented in the model to take into account the non-parabolicity of the conduction band. The energy dependence of the electron effective mass is defined by the following formula:

$$\frac{m_0}{m^*} = \frac{2m_0P^2}{3\hbar^2}\left(\frac{2}{E_g + E} + \frac{1}{E_g + \Delta + E}\right). \tag{2}$$

Here $m_0$ is free electron mass, $P$ is Kane's momentum matrix element, $E_g$ is the band gap, and $\Delta$ is the spin-orbit splitting of the valence band.

Taking into account the relation (2) the Schrödinger equation (1) is expressed as follows

$$(H_{kp}(E) + V_c(\vec{r}))\Psi(\vec{r}) = E\Psi(\vec{r})\,. \tag{3}$$

Here $H_{kp}(E)$ is the single band ***kp***-Hamiltonian operator $H_{kp}(E) = -\nabla\frac{\hbar^2}{2m^*(E,\vec{r})}\nabla$,

$m^*(E,\vec{r})$ is the electron/hole effective mass and $V_c(\vec{r})$ is the band gap potential. As a result, we obtain a non-linear eigenvalue problem.

Solution of the problem (3)-(2) results that the electron/hole effective mass in QD (or QR) varies between the bulk values for effective mass of the QD and substrate materials. The same it is given for the effective mass of carriers in the substrate. The energy of confinement states of carries is rearranged by the magnitude of the band gap potential $V_c$.

The Schrödinger equation (1) with the energy dependence of effective mass can be solved by the iteration procedure (Li et al., 2002; Voss, 2005; Filikhin et al., 2004, 2005).

$$\begin{aligned} &H_{kp}(m^{*k-1}_i)\Psi^k(\vec{r}) = E^k\Psi^k(\vec{r}), \\ &m^{*k}_i = f_i(E^k), \end{aligned} \tag{4}$$

where $k$ is the iteration number, $i$ refers to the subdomain of the system; $i=1$ for the QD, $i=2$ for the substrate. $H_{kp}(m^{*k}_i)$ is the Hamiltonian in which the effective mass does not depend on energy and is equal to the value of $m^{*k}_i$, $f_i$ is the function defined by the relation (2). For each step of the iterations the equation (1) is reduced to Schrödinger equation with the effective mass of the current step which does not depend on energy. At the beginning of iterations the bulk value of the effective mass is employed. Obtained eigenvalue problem can be solved numerically (by the finite element method, for example). After that, a new value for effective mass is taken by using Eq. (2) and procedure is repeated. The convergence of the effective mass during the procedure has a place after 3-5 steps. As an example, the typical convergences for election effective mass and confinement energy of single electron are displayed in Fig. 1 for the InAs/GaAs QR (Filikhin et al., 2005). Description of other methods for the solution of the problem (3)-(2) can be found in (Betcke & Voss, 2011).

Remarks: at the first, in the present review the consideration was restricted by the electron and heavy hole carriers, and, the second, the Coulomb interaction was excluded. Often the linear approximation for the function $m^*_i/m_0 = f(E,r)$ is used. We also will apply the linear fit in the present chapter.

### 2.1.3 Effective approach for strained InAs/GaAs quantum structures: Effective potential

Here we propose the effective potential method to calculate the properties of realistic semiconductor quantum dot/ring nanostructures with the explicit consideration of quantum dot size, shape, and material composition. The method is based on the single sub-band approach with the energy dependent electron effective mass (Eq. (3)). In this approach, the confined states of carriers are formed by the band gap offset potential. Additional effective potential is introduced to simulate the cumulative band gap deformations due to strain and piezoelectric effects inside the quantum dot nanostructure. The magnitude of the effective potential is selected in such a way that it reproduces experimental data for a given nanomaterial.

We rewrite the Schrödinger equation (3) in the following form:

$$(H_{kp}(E) + V_c(\vec{r}) + V_s(\vec{r}))\Psi(\vec{r}) = E\Psi(\vec{r})\,. \tag{5}$$

Here $H_{kp}(E)$, as before, is the single band ***kp***-Hamiltonian operator $H_{kp}(E) = -\nabla \frac{\hbar^2}{2m^*(E,\vec{r})} \nabla$.

As previously, $m^*(E,\vec{r})$ is the electron (or hole) effective mass, and $V_c(\vec{r})$ is the band gap potential, $V_s(\vec{r})$ is the effective potential. $V_c(\vec{r})$ is equal zero inside the QD and is equal to $V_c$ outside the QD, where $V_c$ is defined by the conduction band offset for the bulk (see Section 1.22). The effective potential $V_c(\vec{r})$ has an attractive character and acts inside the volume of the QD. This definition for the effective potential is schematically illustrated by Fig. 2 for the conduction band structure of InAs/GaAs QD. In the figure, the confinement potential of the simulation model with effective potential $V_s$ is denoted as "strained". The band gap potential for the conduction band (valence band) can be determinate as $V_c$ =0.594 eV ($V_c$ =0.506 eV). The magnitude of the effective potential can be chosen to reproduce experimental data. For example, the magnitude of $V_s$ for the conduction (valence) band chosen in (Filikhin et al., 2009) is 0.21 eV (0.28 eV). This value was obtained to reproduce results of the 8-th band ***kp***-calculations of (Schliwa et al., 2007) for InAs/GaAs QD. To reproduce the experimental data from (Lorke et al., 2000), the $V_s$ value of 0.31 eV was used in (Filikhin, et al. 2006) for the conduction band.

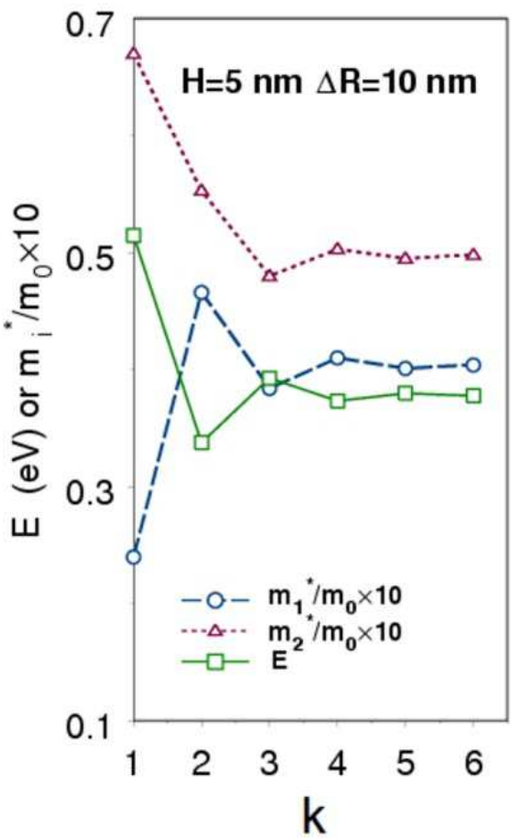


Fig. 1. Convergence of the iterative procedure (4) for the confinement energy $E$ (solid line) and electron effective mass $m^*_i/m_0$ calculated for InAs/GaAs QR (dashed line) and GaAs substrate (dotted line). Here the height of QR is $H$, radial width is $\Delta R$ and inner radius is $R_1$ ($R_1$ =17 nm), $V_c$ =0.77 eV.

Possibility for the substitution of the function describing the strain distribution in QD and the substrate was firstly proposed in (Califano & Harrison, 2000). Recent works (Zhao & Mei, 2011; Li, Bin & Peeters, 2011) in which the strain effect taken into account rigorously applying the analytical method of continuum mechanics allow us to say that the approximation of the effective potential is appropriate.

In the next sub-section of the section 2 we will review the results obtained in both these approximations as the non-parabolic one as well as the effective potential method.

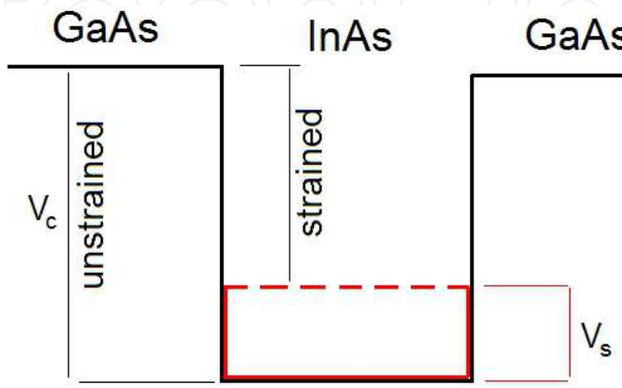


Fig. 2. Effective potential $V_s$ and band gap structure of the conductive band of InAs/GaAs QD.

### 2.2 Electron energy in quantum rings with varieties of geometry: Effect of non-parabolicity

In this section a model of the InAs/GaAs quantum ring with the energy dispersion defined by the Kane formula (2) (non-parabolic approximation) based on single sub-band approach is considered. This model leads to the confinement energy problem with three-dimensional Schrödinger equation in which electron effective mass depend on the electron energy. This problem can be solved using the iterative procedure (4). The ground state energy of confined electron was calculated in (Filikhin et al., 2004, 2005, 2007a) where the effect of geometry on the electron confinement states of QR was studied and the non-parabolic contribution to the electron energy was estimated. The size dependence of the electron energy of QR and QD was subject of several theoretical studies (Li & Xia, 2001; Li et al., 2002). We present here, unlike the previous papers, a general relation for the size dependence of the QR energy.

Consider is semiconductor quantum ring located on the substrate. Geometrical parameters of the semi-ellipsoidal shaped QR are the height $H$, radial width $\Delta R$ and inner radius $R_1$. It is assumed that $H / \Delta R$ << 1 which is appropriate technologically. QR cross section is schematically shown in Fig. 3. The discontinuity of conduction band edge of the QR and the substrate forms a band gap potential, which leads to the confinement of electron.

The band gap potential $V_c(\vec{r})$ is equal to zero inside the QR ($V_c(\vec{r})$ =0) and it is equal to the confinement potential $E_c$ outside of the QR: The spatial dependence of the electron effective mass is given as $m^*(E,\vec{r}) = m_i^*(E)$, $i$ =1,2,3, where $m_1^*$ is the effective mass in the material of QR ($\vec{r}$ $\in$ E1), and $m_2^*(E)$, $m_3^*$ are the effective mass of the substrate material ($\vec{r}$ $\in$ E2 and

E3). Within each of the regions E1, E2 and E3 $m_i^*$ does not depend on the coordinates. The effective mass $m_3^*$ is equal to a constant bulk value. The energy dependence of the electron effective mass from the E1 and E2 subdomains is defined by the formula (2) (Kane, 1957). The equation (1) satisfies the asymptotical boundary conditions: $\Psi(\vec{r})|_{|\vec{r}|\to\infty} \to 0$, $\vec{r} \in$ substrate and $\Psi(\vec{r})|_{|\vec{r}|\in S} = 0$, where $S$ is free surface of QR. On the surface of boundaries with different materials the wave function and the first order derivative $(\vec{n},\vec{\nabla}\Psi)/m_i^*$ are continuous (the surface normal $\vec{n}$).

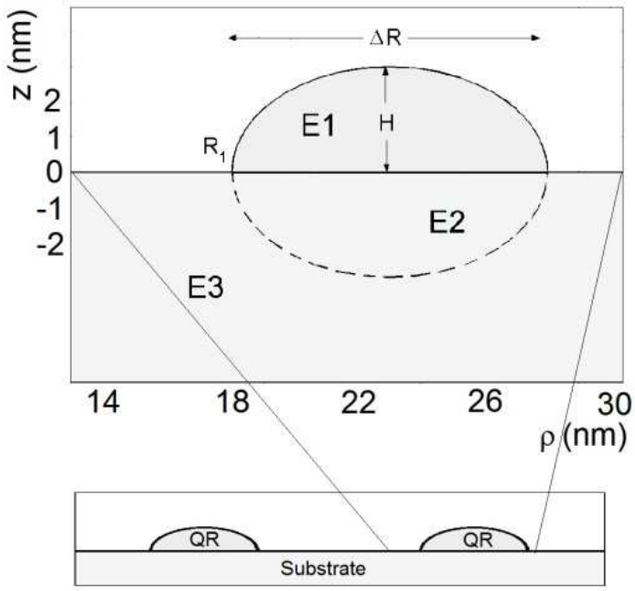


Fig. 3. Profile of cross section of quantum ring (E1) and substrate (E2 and E3). Cylindrical coordinates $\rho$ and z shown on axis.

The Schrödinger equation (3) was numerically solved by the finite element method and iterative procedure (4). The following typical QR/substrate structures with experimental parameters were chosen: InAs/GaAs and CdTe/CdS. The parameters of the model are given in Tabl. 1 for the each hetero-structure.

| QR/Substrate | $m^*_1 / m^*_2$ | $m^*_1 / m^*_2$ (eV) | $\frac{2m_0P_1^2}{\hbar^2} / \frac{2m_0P_2^2}{\hbar^2}$ | $\Delta_1 / \Delta_2$ |
|---|---|---|---|---|
| InAs/GaAs | 0.024/0.067 | 0.77 | 22.4/24.6 | 0.34/0.49 |
| CdTe/CdS | 0.11/0.20 | 0.66 | 15.8/12.0 | 0.80/0.07 |

Table 1. Parameters of the QR and substrate materials

It has to be noted that the effective mass substrate calculated for the InAs/GaAs and CdTe/CdS QRs is slightly differ from the bulk values within area E2. One can consider a simpler model when the properties of the area E2 and E3 are similar. It means that the wave function of electron does not penetrated by surface of QR (area E1) essentially. The simple model does not change qualitative results of these calculations.

Analysis of the results of numerical calculations shows that the ground state energy of QR can be best approximated as a power function of the inverse values of the height and the radial width:

$$E \approx a(\Delta R)^{-\gamma} + bH^{-\beta}, \tag{6}$$

where the coefficients $\gamma$=3/2 and $\beta$=1 were obtained numerically by the least square method. An example of this relation is illustrated in Fig. 4 for InAs/GaAs QR. Parameters a and b remain constant except for extremely low values of $H$ and $\Delta R$. Our analysis also reveals a significant numerical difference between the energy of QR electron ground states, calculated in non-parabolic and parabolic approximations. The results of the calculation with parabolic approximation are represented in the Fig. 4 by the dashed lines. Computation of the electron confinement energy of QRs for different materials shows that the non-parabolic contribution is quite significant when chosen QR geometrical parameters are close to those of the QRs produced experimentally: $H$ < 7 nm, $R$ < 30 nm for InAs/GaAs, $H$ < 5 nm, $R$ < 20 nm for CdTe/CdS. Magnitude of this effect for InAs/GaAs can be greater than 30%. According with this fact the coefficients $a$ and $b$ in Eq. (6) also depend on the approximation used: $a/b$ =3.4/1.9 for the non-parabolic and $a/b$ =6.2/3.0 for parabolic approximation.

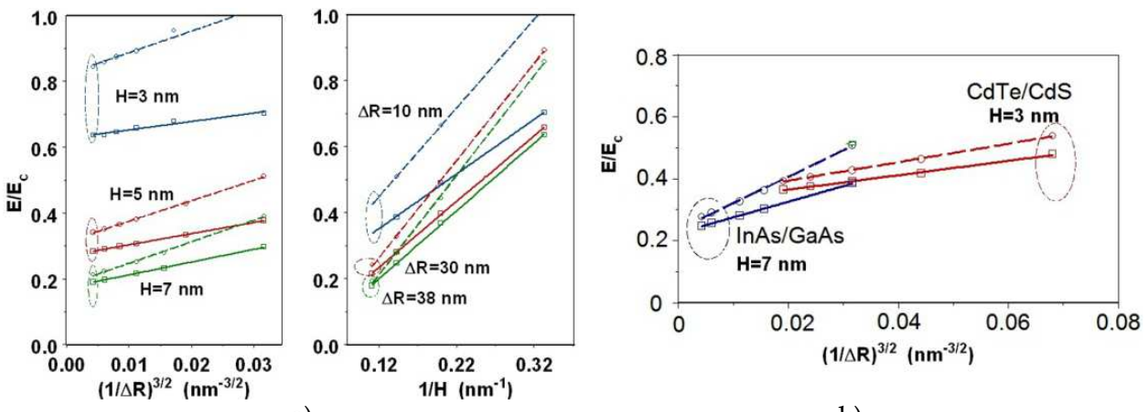


a) b)

Fig. 4. a) Normalized electron ground state energy of semi-ellipsoidal shape InAs/GaAs QR with parabolic (dashed line) and non-parabolic (solid lines) approximation as function of the QR size ($R_1$ =17 nm). b) Normalized electron confinement energy of QRs of various materials in the parabolic (dashed line) and non-parabolic (solid lines) approximation.

As it can be seen from the Fig. 4b), coefficients $\gamma$ and $\beta$ in the relation (6) do not depend on QR/substrate materials. Their values are defined by geometry and by the boundary conditions of the applied model. The model described above corresponds to the boundary condition as "hard wall at one side" (top side of the QR). For the model without the walls when the QR embedded into the substrate one can obtain $\gamma$=1, and $\beta$=1/3. In contrast with it, the coefficients $a$ and $b$ depend on the QR/substrate material set essentially.

Concluding, we have shown that for wide QR sizes the non-parabolicity effect does considerably alter the energy of the electron states, especially when the height or width of QR is relatively small.

### 2.3 The C-V measurements and the effective model: Choosing the parameters

The well-established process of QDs formation by epitaxial growth and consecutive transformation of QDs into InAs/GaAs quantum rings (QR) (Lorke et al., 2000) allows the production of 3D structures with a lateral size of about 40-60 nm and a height of 2-8 nm. In produced QDs and QRs it is possible directly to observe discrete energy spectra by applying capacitance-gate-voltage (CV) and far-infrared spectroscopy (FIR). In this section we will show how the effective model works using as an example the CV data. We use results of the CV experiment from (Lorke et al., 2000; Emperador et al., 2000; Lei et al., 2010) for QD and QR.

The effective mass of an electron in QD and QR is changing from the initial bulk value to the value corresponding to the energy given by the Kane formula (2). Results of the effective model calculations for the InAs/GaAs QR are shown in Fig. 5. The effective mass of an electron in the InAs QR is close to that of the bulk value for the GaAs substrate. Since the effective mass in the QD is relatively smaller, as it is clear from Fig. 5, for QD the electron confinement is stronger; the $s$-shell peak of the CV trace is lower relative upper edge of conduction band of GaAs. The lower $s$-shell peak corresponds to the tunneling single electron into the QD. The pictures is a starting point for the choosing the parameters of the effective potential model. In this section we follow the paper (Filikhin et al., 2006a) where the semi-ellipsoidal InAs/GaAs QD has been considered. The average sizes of InAs/GaAs QD reported in (Lorke et al., 2000) were: $H$ =7 nm (the height) and $R$ =10 nm (the radius). A cross section of the quantum dot is shown in Fig. 6a). The quantum dot has rotation symmetry. Thus the cylindrical coordinate was chosen in Eq. (5) which defines the effective model. For each step of iterative procedure (4) the problem (3-2) is reduced to a solution of the linear eigenvalue problem for the Schrödinger equation.

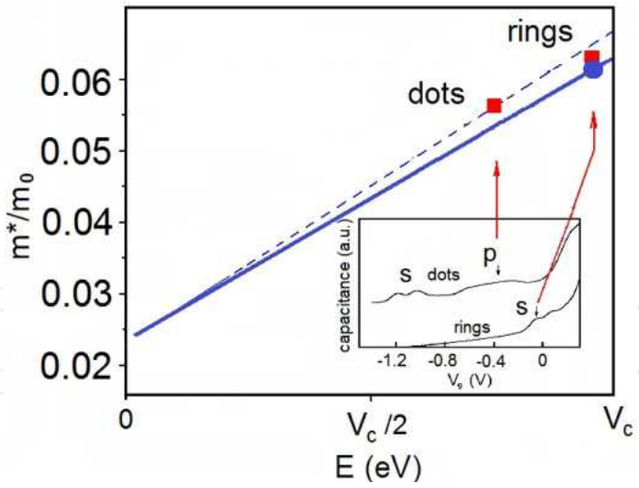


Fig. 5. Calculated (circle) and experimentally obtained by (Lorke et al., 2000; Emperador et al., 2000) (squares) values for the electron effective mass and the confinement energies of the electron $s$- and $p$-levels of QD and QR. The solid line is obtained by the Kane formula (2), and the dashed line connects the bulk values of the effective mass. The insert: the capacitance-gate voltage traces (Lorke et al., 2000).

Taking into account the axial symmetry of the quantum dot (ring) considered, this equation may be written in the cylindrical coordinates $(\rho, z, \phi)$ as follows:

$$(-\frac{\hbar^2}{2m^*}(\frac{\partial^2}{\partial\rho^2}+\frac{1}{\rho}\frac{\partial}{\partial\rho}-\frac{l^2}{\rho^2}+\frac{\partial^2}{\partial z^2})+V_c(\rho,z)+V_s(\rho,z)-E)\Phi(\rho,z)=0. \quad (7)$$

The wave function is of the form: $\Psi(r)=\Phi(\rho,z)exp(il\phi)$, where $l$=0, $\pm1$, $\pm2\ldots$ is the electron orbital quantum number. For each value of the orbital quantum number $l$, the radial quantum numbers $n=0,1,2,...$ are defined corresponding to the numbers of the eigenvalues of (4) which are ordered in increasing. The effective mass $m^*$ must be the mass of electron for QD or for the substrate depending on the domain of the Eq. (3) is considered.

The wave function $\Phi(\rho,z)$, and its first derivative in the form $\frac{\hbar^2}{2m^*}(\vec{n},\nabla)\Phi$, have to be continuous throughout the QD/substrate interface, where $\vec{n}$ is the normal vector to the interface curve. The Neumann boundary condition $\frac{\partial}{\partial\rho}\Phi(\rho,z)=0$ is established for $\rho=0$.

The asymptotical boundary conditions is $\Phi(\rho,z)\to0$, when $\rho\to\infty$, $|z|\to\infty$ (QD is located near the origin of z-axes).

When quantum dots are in an external perpendicular magnetic field, as it will be considered below, the magnetic potential term must be added to the potentials of Eq. (7) (Voskoboinikov et al., 2000) in the form $V_m(\rho)=\frac{1}{2m^*}(\beta\hbar l+\frac{\beta^2}{4}\rho^2)$, where $\beta=eB$, $B$ is the magnetic field strength, and $e$ is the electron charge. We consider the case of a magnetic field normal to the plane of the QD and do not take into account the spin of electron because the observed Zeeman spin-splitting is small.The confinement potential in Eq. (7) was defined as follows: $V_c$ = 0.7($E_g^S-E_g^{QD}$); $V_c$ = 0.77 eV. The parameters of the QD and substrate materials were $m^*_{bulk,1}/m^*_{bulk,2}$ =0.024/0.067, $E_g^{QD}/E_g^S$ =0.42/1.52, $\frac{2m_0P_1^2}{\hbar^2}/\frac{2m_0P_2^2}{\hbar^2}$ =20.5/24.6, $\Delta_1/\Delta_2$ =0.34/0.49. The magnitude of the effective potential $V_s$ was chosen as 0.482 eV. There are three electron confinement states: the $s$, $p$, and $d$, as shown in the Fig. 6b). The energy of the $s$ single electron level measured from the top of the GaAs conduction band can be obtained from CV experimental data. To explain it, in Fig. 6c) the capacitance-gate-voltage trace from (Miller et. al., 1997) is shown. The peaks correspond to the occupation of the $s$ and $p$ energy shells by tunneled electrons. The Coulomb interaction between electrons results to the $s$-shell splits into two levels and the $p$-shell splits into four levels taking into account the spin of electron and the Pauli blocking for fermions. The gate voltage-to-energy conversion coefficient $f=7$ ($\Delta E=e\Delta V_g/f$) was applied to recalculate the gate voltage to the electron energy. The value of the effective potential $V_s$ was chosen in order to accurately reproduce the observed $s$-wave level localization with respect to the bottom of GaAs conduction band. The approximate size of this energy region is 180 meV.

The non-parabolic effect causes a change in the electron effective mass of QD with respect to the bulk value. According to the relation Eq. (2), the effective electron mass for InAs is sufficiently increased from the initial value of $0.024\,m_0$ to $0.054\,m_0$, whereas for GaAs

substrate it is slightly decreased from $0.067\,m_0$ to $0.065\,m_0$ within the region where the wave function is out of the quantum dot. The obtained value of the electron effective mass of InAs in QD is close to the one ($0.057\,m_0 \pm 0.007$) extracted in (Miller et. al., 1997) from the CV measurements of orbital Zeeman splitting of the $p$ level.

Appling the obtained effective model, one can take into account the effect the Coulomb interaction between electrons (the Coulomb blockade). The goal is to reproduce the C-V data presented in Fig. 6 for the InAs QD. The calculations (Filikhin et al., 2006a) have been carried out using the perturbation procedure, proposed in (Warburton et al., 1998). The Coulomb energy matrix elements were calculated by applying single electron wave functions obtained from the numerical solution of Eq. (7). Both the direct terms of $E_{ij}^{c}$ and the exchange terms $E_{ij}^{x}$ of the Coulomb energy between electron orbitals with angular momentum projection of $\pm i$ and $\pm j$ were calculated (notation is given in (Warburton et al., 1998)). The results of calculations of the electron energies of the $s$, $p$ and $d$ levels are shown in Fig. 7 ($Cal.\,2$). The $s$ shell Coulomb energy was found to be close to the experimental value which is about 20 meV.

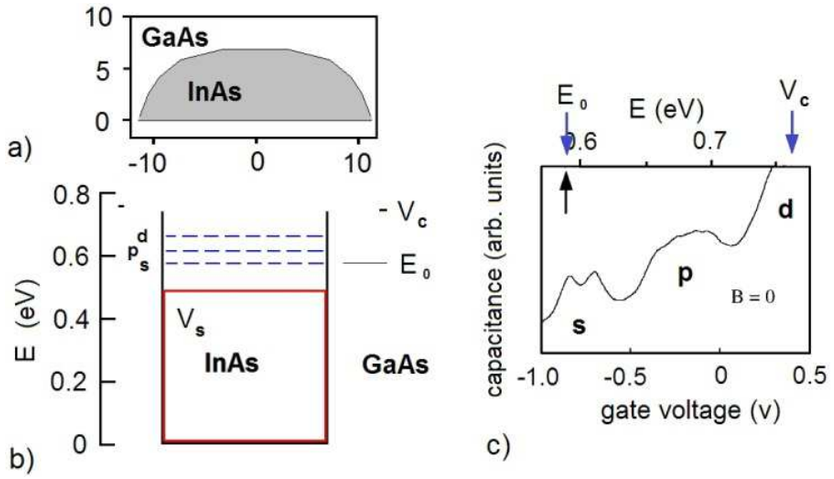


Fig. 6. a) A cross section of the quantum dot. The dimensions are given in nm. b) Localization of the $s$, $p$ and $d$ single electron levels relatively to the bottom of the GaAs conduction band. $V_c$ is the band-gap potential, $V_s$ is the effective potential simulating the sum of the band-gap deformation potential, the strain-induced potential and the piezoelectric potential. c) The capacitance-gate-voltage trace (Miller et. al., 1997). The peaks correspond to the occupation of the $s$ and $p$ energy shells by tunneled electrons. The arrows denote the $s$ level ($E_0$) and the bottom of the GaAs conduction band.

Returning to the Fig. 5 we have to note that the effective potential obtained for InAs/GaAs QD has to be corrected for the case of the InAs/GaAs quantum rings. The reason is the topological, geometrical dependence of the depth of the effective potential. This dependence is weak for the considered QD and QR. The corresponding $V_s$ potentials have the magnitude of 0.482 eV and 0.55 eV for QD and QR, respectively. Accordingly to the experimental data the electron effective mass in quantum dots and rings is changing from $0.024\,m_0$ to $(0.057 \pm 0.007)\,m_0$ (Miller et. al., 1997) and $0.063\,m_0$ (Lorke et al., 2000), respectively. The Kane's formula describes these variations well as it is shown in Fig. 5. The

calculated values for the effective masses for quantum dots and rings are $0.0543\,m_0$ and $0.0615\,m_0$, respectively (Filikhin et al., 2006).

Correct choice of the average QD profile is important for an analysis of the C-V data. It was shown in (Filikhin et al., 2008), where the calculation of the energy shifts due to the Coulomb interaction between electrons tunneling into the QD was performed for comparison with the C-V experiments.

One can see in Fig. 7 that the agreement between our results and the experimental data is satisfactory well. Slight disagreement can be explained by uncertainty in the QD geometry which has not been excluded by available experimental data. In (Filikhin et al., 2008) it was shown that small variations of the QD cross section lead to significant changes in the levels presented in Fig. 7. The variations of the QD profile we considered are shown in Fig. 8a, and the results of calculations for the electron energies are presented in Fig. 8b) for $s$, $p$ and $d$ –shell levels. The results of the calculations shown in Fig. 8 reveal rather high sensitivity to these variations of the QD profile. In particular, the spectral levels shift is noticeable due to a small deformation of the QD profile. Thus, we have seen that the average QD profile is important when we are comparing the result of the calculations and the experimental data.

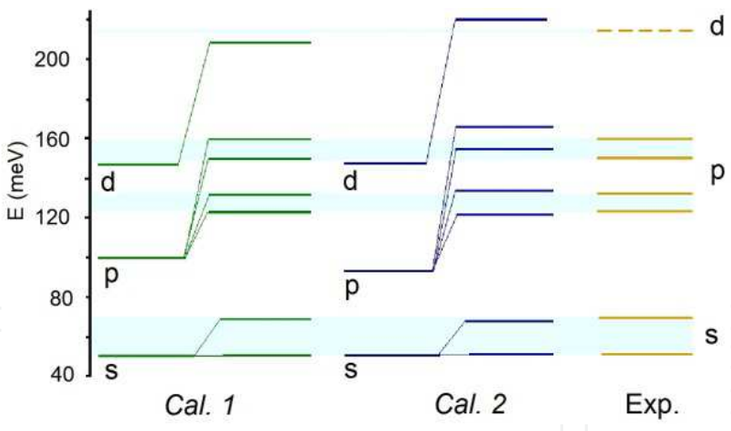


Fig. 7. Energies of the electrons occupying a few first levels of the quantum dot at zero magnetic field. The calculations *Cal*. 1 are that of parabolic model (Warburton et al., 1998). Our calculations are denoted by *Cal*. 2. The splitting of the single electron levels of a corresponding energy shell is presented. CV experimental data are taken from (Warburton et al., 1998).

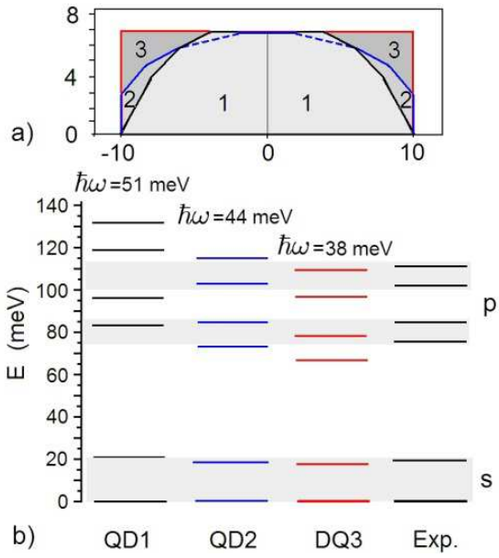


Fig. 8. a) Cross sections of the QD. The dimensions are given in nm. b) Excitation energies of the electrons occupying $s$ and $p$ -energy shells of the InAs/GaAs quantum dot for various QD profiles are shown in Figure 7a). CV experimental data are taken from (Warburton et al., 1998). Here $\hbar\omega$ is the excitation energy $\hbar\omega = E_{(0,0)} - E_{(0,1)}$, where $E_{(n,l)}$ is a single electron energy of the $(n,l)$ state.

Finally, we may conclude that the effective model of QD/substrate semiconductor structure with the energy dependent effective mass and realistic 3D geometry taken into account, can quantitatively well interpret the CV spectroscopy measurements.

### 2.4 Electron effective mass in the InAs/GaAs QD

In this section we present the effective model based on another version of the band structure model for InAs/GaAs QDs proposed in (Filikhin et al., 2008). The cross section of the semi-ellipsoidal shaped InAs QD embedded in a GaAs substrate is shown in Fig. 6a). Band gap structure model was defined by choosing for the conduction band $\kappa^{CB}$ =0.54, and for the valence band $\kappa^{VB}$ =0.46 (Duque et al., 2005). Using experimental values $E_{g,1}$ =0.42 eV, $E_{g,2}$ =1.52 eV we obtain $V_c$ =0.594 eV for the conduction band and. $V_c$ .=0.506 eV for the valence band. The band structure model for InAs/GaAs QDs is shown in Fig. 9.

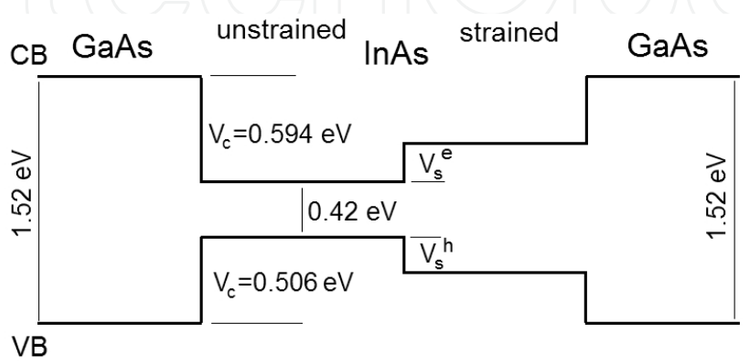


Fig. 9. Band structure model for InAs/GaAs QDs. CB (VB) is conduction (valence) band.

Bulk effective masses of InAs and GaAs are $m^*_{0,1}$=0.024 $m_0$ and $m^*_{0,2}$=0.067 $m_0$, respectively. For the effective mass of the heavy hole, a value of $m^*$=0.4 $m_0$ for both the QD and the substrate was used. The band gap model just described is for "unstrained" InAs/GaAs structures. Realistic models for QDs must take into account the band-gap deformation potential, the strain-induced potential, and the piezoelectric potential, in addition to the band-gap potential. These effects can be included by introducing an effective potential $V_s$. The magnitude of the potential has been chosen (Filikhin et al., 2006) to reproduce experimental data and the value of 0.31 eV was used for $V_s$. The effect of non-parabolicity, taken into account in the effective model, leads to a change of the effective electron mass in the QD relative to its bulk value. For the QD under study, the effective mass for InAs increases from the initial bulk value of 0.024 $m_0$ to 0.057 $m_0$ which coincides with the experimental value $0.057m_0 \pm 0.007m_0$, obtained in CV measurements through the Zeeman splitting of $p$-shell levels. This result is shown in Fig. 10. In accordance with Eqs. (2)-(3), the effective electron masses in the $s$, $p$ and $d$ states are different. The value of the effective mass, mentioned

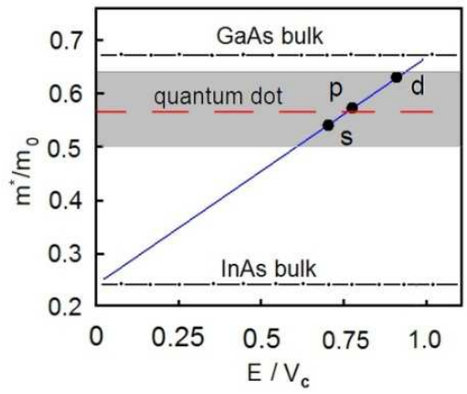


Fig. 10. Effective mass of electron and single electron energy of $s$, $p$, $d$-levels in InAs/GaAs QD. Dashed line corresponds to the experimental value. The grey color stripe shows the experimental uncertainty.

above, corresponds to the one for the $p$-state. The effective mass for $s$-shell is slightly less and is equal to 0.054 $m_0$. The differences of the effective masses are small and cannot be extracted from this experiment due to the large experimental uncertainties (Miller et al., 1998).

### 2.5 Experimental data for InAs/GaAs QR and the effective model

In this section we continue the description of the effective model use on the example of InAs/GaAs quantum ring. The geometry of the self-assembled QRs, reported in (Lorke et al., 2000), is shown in Fig. 11 (Geometry 1). The InGaAs QRs have a height of about 2 nm, an outer diameter of about 49 nm, and an inner diameter of about 20 nm. Also, three-dimensional QR geometry (Geometry 2), which follows from the oscillator model (Lei et al., 2010) is used. The confinement of this model is given by the parabolic potential:

$U(r) = \frac{1}{2} m^* \omega (r - r_0)^2$, where $\omega$, $r_0$ are parameters (Chakraborty & Pietiläinen, 1994). The QR geometry is dictated by the relation between the adopted oscillator energy and a length $l$ as follows (Szafran & Peeters, 2005):

$$l = \sqrt{2\hbar / m^* \omega}\,. \tag{8}$$

Here the width $d$ for the considered rings is defined by $d = 2l$. The obtained geometry with the parameters $m^*$ and $\omega$ from (Lei et al., 2010) is shown in Fig. 11 (Geometry 2); $m^*$=0.067 $m_0$ and $\omega$=15 meV. The center radius of QR is 20 nm.

Results of the effective model calculations for the ground state energy of electron in a magnetic field are shown in Fig. 12. (Filikhin et al. 2011a) The picture of the change of the orbital quantum number of the ground state is similar to that obtained in (Lei et al., 2010) with the oscillator model. The change occurred at 2.2 T and 6.7 T. The obtained energy fits the experimental data rather well.

It has to be noted here that one cannot reproduce this result using the geometry proposed in (Lei et al., 2010) (Geometry 1) for this QR. The correspondence between the confinement potential parameters of the oscillator model and the real sizes of quantum objects has to be established by Eq. (8). Only using the geometry followed from Eq. (8) we reproduce result of (Lei et al., 2010), as is shown in Fig. 12. The strength parameter of the effective potential, in the case of the Geometry 2, was chosen to be 0.382 eV, which is close to that for QD from (Filikhin et al., 2008), where $V_s$ =0.31 eV. The difference is explained by the topology dependence of the effective potentials (see section above and also (Filikhin et al., 2006)).

Note that the considered QRs are the plane quantum rings with the condition $H$ <<D (for height and diameter of QR), which enhances the role of the lateral size confinement effect. To qualitatively represent the situation shown in Fig. 12, one can used an approximation for the 3D QR based on the formalism of one dimensional ideal quantum ring. Additional electron energy, due to the magnetic field, can be calculated by the relation: $E = \hbar^2 / (2m^* R^2)(l + \Phi / \Phi_0)^2$ (see for instance (Emperador et al., 2000)), where fluxes are $\Phi = \pi R^2 B$, $\Phi_0 = h / e$ .. ($\Phi_0 = 4135.7$ T nm²); $R$ is radius of the ideal ring. The Aharonov-Bohm (AB) (Aharonov & Bohm, 1959) period $\Delta B$ (Aronov & Sharvin, 1987) is given by the relation: $\Delta B = \Phi_0 / \pi / R^2$. Using the root mean square (rms) radius for $R$ ($R$ =20.5 nm), one can obtain $\Delta B / 2$ =1.56 T and $\Delta B / 2 + \Delta B$ =4.68 T for the ideal ring. This result is far from the result of 3D calculations shown in Fig. 12 where $\Delta B / 2 \approx 2.2$ T and $\Delta B / 2 + \Delta B \approx 6.7$ T are determined. Note here that the electron root mean square radius $R_{n,l}$ is defined by the relation $R^2_{n,l} = \int |\Phi^N_{n,l}(\rho, z)|^2 \rho^3 d\rho dz$, where $\Phi^N_{n,l}(\rho, z)$ is the normalized wave function of electron state described by the quantum numbers $(n, l)$.

One can obtain better agreement by using the radius for the most probable localization of the electron $R_{loc.}$, defined at the maximum of the square of the wave function. The electron is mostly localized near 17.1 nm, for $B$ =0. With this value, the ideal ring estimation leads to the values for $\Delta B / 2$ and $\Delta B / 2 + \Delta B$ as 2.25 T and 6.75 T, respectively. That agrees with the result of the 3D calculations (see Fig. 12). Obviously, the reason for this agreement is the condition $H << D$, for the considered QR geometry as it was mentioned above. The mostly localized position of the electron in QR depends weakly on the magnetic field. We present .. as a function of the magnetic field $B$ in Fig. 13. $R_{loc.}(B)$ is changed in an interval of ±1 nm

around the mean value $R_{loc.}(0)$ of 17 nm. It is interesting to note that the magnetization of a single electron QR demonstrates the same behavior as it does for $R_{loc.}(B)$ if the one dimensional ring is used (see (Voskoboynikov et al., 2002) for details).

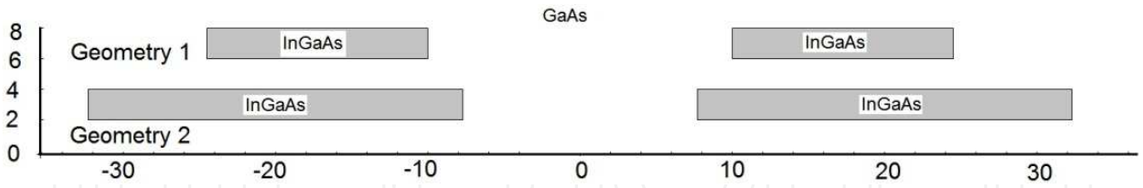


Fig. 11. QR cross section profile corresponding to Geometry 1 and Geometry 2; sizes are in nm.

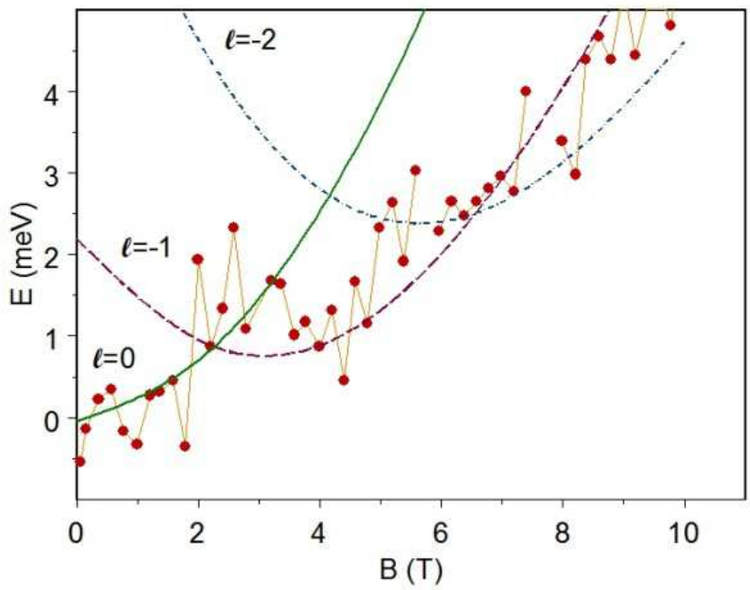


Fig. 12. Additional energy of an electron in QR in a magnetic field $B$. The C-V experimental energies (circles) were obtained in (Lei, et al. 2010) by using a linear approximation $\Delta E = e\Delta V_g / f$, with the lever arm $f = 7.84$. The curves $l = 0, -1, -2$ are the results of our calculations multiplied by a factor of 1.18 (Lei, et al. 2010).

Additionally we compare the results of calculations for the QR geometry parameters corresponding to Geometry 1 and Geometry 2 in Fig. 11 with the far-infrared (FIR) data, reported in (Emperador, et al. 2000). The results are presented in Fig. 14. One can see that the QR geometry proposed in (Lei et al., 2010) leads to a significant difference between the FIR data and the effective model calculations (see Fig. 14a), whereas the results obtained with Geometry 2 are in satisfactory agreement with the data (Fig. 14b). Again we conclude that the QR geometry of (Lei et al., 2010) does not provide an adequate description of electron properties of the InAs/GaAs QRs measured in (Lorke et al., 2000; Lei et al., 2010).

To summarize, we wish to point out that the problem of reliable theoretical interpretation of the C-V (and FIR) data for InAs/GaAs quantum rings is far from resolved. Obtained geometry can be considered as a possible version of geometry for experimentally fabricated QR.

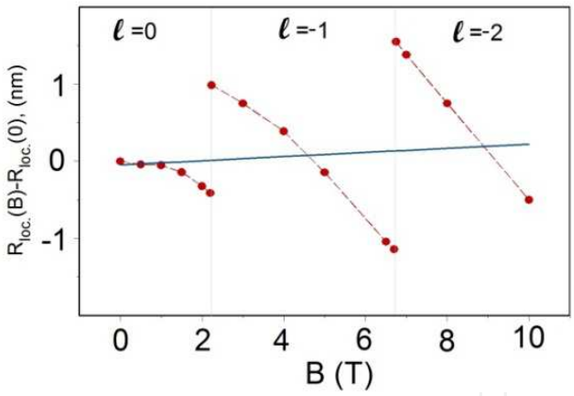


Fig. 13. The radius ( $R_{loc.}$ ) of the most localized position of an electron as a function of a magnetic field $B$. The electron of the ground state is considered. The circles indicate the calculated values and the solid line indicates the result of the least squares fitting of the calculated values. The orbital quantum number of the ground state is shown.

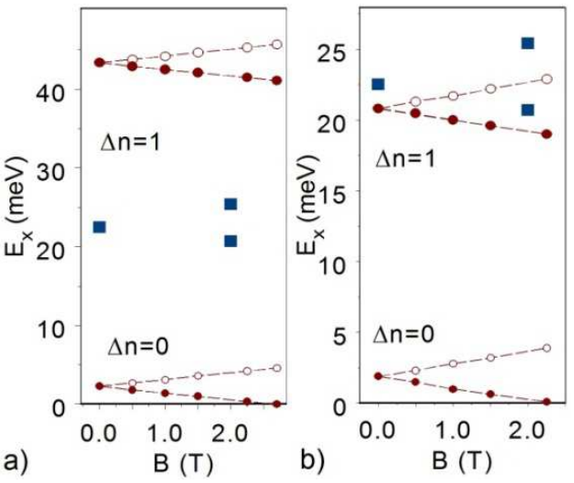


Fig. 14. Solid squares represent the observed resonance positions (Emperador, et al. 2000) of the FIR transmissions at various magnetic field $B$. Calculated energies of the excited states with $|\Delta l|=1$ are marked by the circles. a) QR with shape given by Geometry 1, b) QR with shape given by Geometry 2. The orbital quantum number of the ground state is $l=0$. The quantum number $n$ is changed as shown.

### 2.6 Material mixing in InGaAs/GaAs quantum dots

The fabrication process of nano-sized self-assembled InAs/GaAs quantum dots and quantum rings may be accompanied by the material mixing in the initially pure InAs QDs due to interdiffusion of the QD/substrate materials. This mixing cannot be precisely controlled, resulting in QDs with spatially inhomogeneous Ga fractions that are not well specified. In this section we show an application of the effective model to study $In_xGa_{1-x}As$ QDs with significant Ga fractions.

InAs QDs having a semi-ellipsoidal shape embedded into the GaAs substrate are considered (see Fig. 6a)). The effective potential $V_s$ =0.31 eV, which was found in (Filikhin et al., 2008)

for pure InAs QDs, reproduces the capacitance-gate-voltage experiments satisfactory well (in Table 2 these results described in the column "0% Ga ($V_s$ =0.31eV)"). It was assumed that a realistic approach must therefore take into account material mixing. The results of the effective model calculations for Ga fractions of 10%, 20% and 25% are listed in Table 2 (Filikhin et al., 2009). The calculations was performed varying the Ga fraction in QDs for strength parameters $V_s^e$ =0.21 eV and $V_s^h$ =0.28 eV of the potential. The effective electron mass, the band gap and the effective potential for $In_xGa_{1-x}As$ changed linearly with respect to the value of the Ga fraction, assuming a homogeneous distribution of Ga in the QD volume. The experimental value of the transition energy for recombination of an exciton pair ($E_{ex}$) in the ground state is matched by calculations corresponding to a Ga fraction of approximately 22% in the QDs. Thus we conclude that the data obtained in CV and PLexperiments to this QD may be related with mixing in QD of 22%. It has to note that calculations with the 22% in the QDs ($V_s$ =0.21eV) and pure InAs QDs (used $V_s$ =0.31eV) demonstrate some uncertainties in the QD geometry and the Ga fraction and may lead to non-unique descriptions of the same experimental data.

| Ga fraction | 10% | 20% | 25% | 0% ($V_s$ =0.31eV) | Exp. |
|---|---|---|---|---|---|
| $m^*/m_0$ | 0.050 | 0.056 | 0.057 | 0.057 | $0.057 \pm 0.007$ |
| $\Delta E(e)$ $\Delta E(h)$ | 238<br>245 | 205<br>217 | 188<br>151 | 185<br>206 | <br>204 |
| $e_1-e_0$ $e_2-e_1$ | 50<br>55 | 48<br>53 | 46<br>52 | 46<br>52 | 44<br>49 |
| $h_0-h_1$<br>$h_1-h_2$ | 10<br>12 | 10<br>11 | 9<br>11 | 10<br>11 | |
| $E^c_{e0e0}$ | 21.0 | 20.9 | 20.8 | 20.8 | 21.5 (or 18.9) |
| $E^c_{e0e1}$ | 18.1 | 18.0 | 17.9 | 18.0 | 24 (or 13.0) |
| $E^c_{e1e1}$ | 17.0 | 17.0 | 16.9 | 17.0 | ~18.0 |
| $E^c_{h0h0}$ | 25.1 | 24.9 | 24.7 | 25.1 | 24 |
| $E^c_{e0h0}$ | 22.8 | 22.6 | 22.5 | 22.7 | 33.3 |
| $E_{ex}$ | 1014 | 1075 | 1160 | 1106 | 1098 |
| $d_{00}$ | 0.08 | 0.08 | 0.08 | 0.08 | $0.4 \pm 0.1$ |

Table 2. Calculated single electron (hole) energy-level spacing $e(h)$, electron (hole) binding energy $\Delta E(e)$ ($\Delta E(h)$), electron-electron, electron-hole and hole-hole Coulomb energies $E^c_{\alpha\beta}$ ($\alpha,\beta = e,h$), excitonic band gap $E_{ex}$ (in meV), exciton dipole moment $d_{00}$ (in nm) and effective mass of the QD material for semi-ellipsoidally shaped InGaAs QDs (Ga fraction in %) embedded in GaAs. Electron (hole) energy of the ground state is measured from the GaAs conduction (valence) band. The value of the effective mass is given for the $p$-wave electron level.

In (Filikhin et al. 2009) it was brought argument for existence of the essential mixing of the Ga-fraction in QD. The effective model with the material mixing was tested by comparison with available experimental data for the Coulomb shifts of the transition energies for positive ( $X^+$ ) and negative ( $X^-$ ) charged trions and biexcitons ( $XX$ ) as a function of the neutral exciton ( $X$ ) recombination energy. Results of these calculations for various base size parameters of QDs are depicted in Fig. 15, along with experimental data. The root mean square fit of the experimental data from (Rodt et al., 2005) shown by the dashed lines in Fig. 15. The vertical line shows the transition energy that corresponds to the limit of the QD sizes for which there are only two electron and two heavy hole levels. In this case the Coulomb shifts are calculated by combinations of the Coulomb energies of electron-electron, electron-hole and hole-hole pairs:

$$E(XX)-(X)=E^c_{ee}-E^c_{eh}+E^c_{hh}-E^c_{eh},\ E(X^-)-(X)=E^c_{ee}-E^c_{eh},\ E(X^+)-(X)=E^c_{hh}-E^c_{eh}.$$

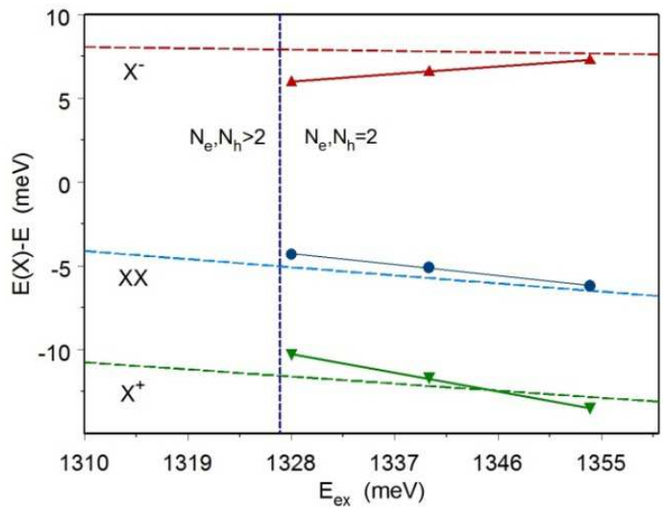


Fig. 15. Coulomb shifts of transition energies for positively ( $X^+$ ) and negatively ( $X^-$ ) charged trions and biexcitons ( $XX$ ) as a function of neutral exciton ( $X$ ) recombination energy. Results of the calculations for various base size parameters of QDs are marked by solid triangles ( $X^-$ , $X^+$ ) and dots ( $XX$ ). The dashed lines correspond to root mean square fits to experimental data from (Rodt et al., 2005). The solid lines correspond to root mean square fits to the calculated results. The vertical line shows the transition energy, which corresponds to the limit of the QD sizes for which there are only two electrons and two heavy holes levels. The amount of the Ga fraction in our calculations is equal to 25%.

When there are several interacting carrier pairs, the calculations must be performed with more intricate scheme using perturbation theory. The value of the Ga fraction in our calculations was 25%. Calculations were performed for three QD geometries. A lens-shaped geometry with a height of 3.5 nm and base sizes of 9 nm, 10 nm and 11 nm were used. The effective model results in Fig. 15 demonstrate qualitative agreement with the experimental data for the aforementioned confinement region. The calculated results are very sensitive to the value of the Ga fraction. In particular, increasing the fraction shifts the $X^+$ and $X^-$ energies to the region of large exciton energies ( $X$ ). At the same time, the Coulomb shifts decrease in absolute value within the region of the $X$ -energies with $N_h$ =2. Decreasing the Ga fraction gives the opposite results.

We can conclude that in the framework of an effective model one can reproduce the CV and PL experimental data for InGaAs/GaAs QDs. In these calculations the amount of the Ga-fraction was taken to be about 22%. Taking into account this value for Ga-fraction we also reproduce the measured transition energies and Coulomb shifts for excitonic complexes ( $X^-$ , $X^+$ , $XX$ ) in the limit of two interacting pairs of carriers in the QDs.

## 3. Quantum chaos in single quantum dots

### 3.1 Quantum chaos

Quantum Chaos concerns with the behavior of quantum systems whose classical counterpart displays chaos. It is quantum manifestation of chaos of classical mechanics.

The problem of quantum chaos in meso - and nano-structures has a relatively long history just since these structures entered science and technology. The importance of this problem is related to wide spectrum of the transport phenomena and it was actively studied in the last two decades (Beenakker & van Houten, 1991; Baranger & Stone, 1989; Baranger et al., 1991). One of the main results of these studies, based mainly on the classical and semi-classical approaches, is that these phenomena sensitively depend on the geometry of these quantum objects and, first of all, on their symmetry: Right - Left (RL) mirror symmetry, up-down symmetry and preserving the loop orientation inversion symmetry important in the presence of the magnetic field (Whitney et al., 2009; Whitney et al., 2009a).

These results are well -known and discussed widely. There is another, actively studied in numerous fields of physics, aspect which ,in essence, is complimentary to the above mentioned semi classical investigations: Quantum Chaos with its inalienable quantum character , including, first of all, Nearest Neighbor level Statistics (NNS ) which is one of the standard quantum-chaos test.

Mathematical basis of the Quantum Chaos is a Random Matrix Theory (RMT ) developed by Wigner, Dyson, Mehta and Goudin (for comprehensive review see book (Beenakker & van Houten, 1991)). RMT shows that the level repulsion of quantum systems (expressed by one of the Wigner-Dyson -like distributions of RMT) corresponds to the chaotic behavior and, contrary, level attraction described by Poisson distribution tells about the absence of chaos in the classical counterpart of the quantum system. This theorem-like statement checked by numerous studies in many fields of science. For the completeness, we add that there are other tests of Quantum Chaos based on the properties of the level statistics: $\Delta_3$ statistics (spectral rigidity $\Delta_3(L)$ ), Number variance $\Sigma_2(L)$ ), spectral form-factor, two- and multipoint correlation functions, two level cluster function $Y_2(E)$ etc. They play an important subsidiary role to enhance and refine the conclusions emerging from the NNS.

The present review surveys the study of the NNS of nanosize quantum objects - quantum dots (QD) which demonstrate atom-like electronic structure under the regime of the size confinement. To use effectively NNS, we have to consider so called weak confinement regime where the number of levels can be of the order of several hundred. QD of various shape embedded into substrate are considered here under the effective model (Filikhin et al., 2010). We use the sets of QD/substrate materials ( $Si/SiO_2$, $GaAs/Al_{0.7}Ga_{0.25}As$, GaAs/InAs).

### 3.2 The nearest neighbor spacing statistics

For the weak confinement regime (for the $Si/SiO_2$ QD, the diameter $D \geq 10$ nm), when the number of confinement levels is of the order of several hundred (Filikhin et al. 2010), we studied NNS statistics of the electron spectrum. The low-lying single electron levels are marked by $E_i$, $i = 0,1,2,...N$. One can obtain the set $\Delta E_i = E_i - E_{i-1}$, $i = 1,2,3,...N$ of energy differences between neighboring levels. An example of the energy spectrum and set of the neighbor spacings for $Si/SiO_2$ QD are in Fig. 16. We need to evaluate the distribution function $R(\Delta E)$, distribution of the differences of the neighboring levels. The function is normalized by $\int R(\Delta E) d\Delta E = 1$. For numerical calculation, a finite-difference analog of the distribution function is defined by following relation:

$$R_j = N_j / H_{\Delta E} / N, \; j = 1,...M,$$

where $\sum N_j = N$ represents total number of levels considered, $H_{\Delta E} = ((\Delta E)_1 - (\Delta E)_N) / M$ is the energy interval which we obtained by dividing the total region of energy differences by $M$ bins. $N_j$ ($j = 1,2,...M$) is the number of energy differences which are located in the $j$ -th bin.

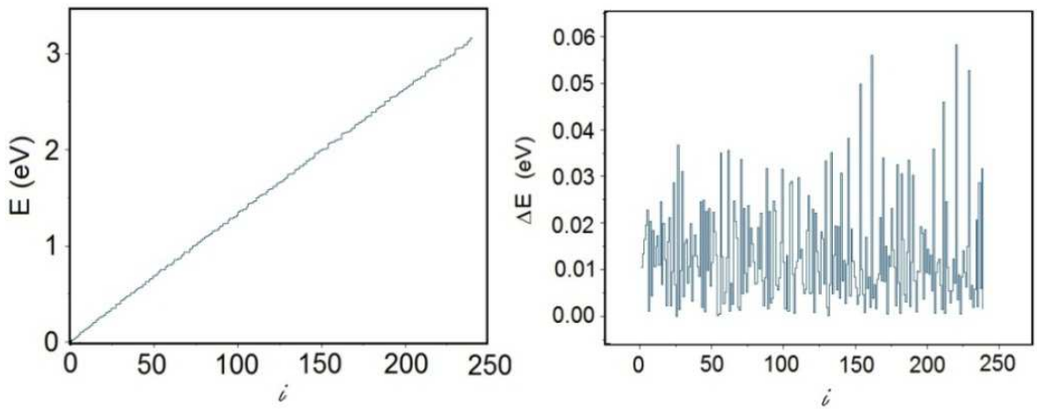


a) b)

Fig. 16. a) The energy levels and b) the neighbor spacings $\Delta E_i = E_i - E_{i-1}$, $i = 1,2,..N$ ,of the spherical $Si/SiO_2$ QD with diameter D=17 nm.

The distribution functions $R(\Delta E)$ is constracted using the smoothing spline method. If $R_j$, $j = 1,2,..M$, are calculated values of the distribution functions corresponding to $\Delta E_j$, the smoothing spline is constructed by giving the minimum of the form $\sum_{j=1}^{M} (R_j - R(\Delta E_j))^2 + \int R''(\Delta E)^2 d(\Delta E) / \lambda$. The parameter $\lambda > 0$ is controlling the concurrence between fidelity to the data and roughness of the function sought for. For $\lambda \to \infty$ one obtains an interpolating spline. For $\lambda \to 0$ one has a linear least squares approximation.

We studied neighbouring level statistics of the electron/hole spectrum treated by way considered above. The Si quantum dots having strong difference of electron effective mass in two directions is considered as appropriate example for the study of role of the effective mass asymmetry. In this study we do not include the Coulomb potential between electrons and holes. The shape geometry role is studied for two and three dimensions.

### 3.3 Violation of symmetry of the QD shape and nearest neighbor spacing statistics

Distribution functions for the nearest neighboring levels are calculated for various QD shapes (Filikhin et al., 2010). Our goal here to investigate the role of violation of the symmetries of QD shape on the chaos. The two and three dimensional models are considered. Existing of any above mentioned discrete symmetry of QD shape leads to the Poisson distribution of the electron levels.

In Fig. 17 the numerical results for the distribution functions of $Si/SiO_2$ QD are presented. The QD has three dimensional spherically shape. We considered the two versions of the shape. The first is fully symmetrical sphere, and the second shape is a sphere with the cavity damaged the QD shape. The cavity is represented by semispherical form; the axis of symmetry for this form does not coincide with the axis of symmetry of the QD. In the first case, the distribution function is the Poisson-like distribution. The violation symmetry in the second case leads to non-Poisson distribution.

We fit the non-Poissonian distribution function $R(\Delta E)$ using the Brody distribution (Brody et al., 1999):

$$R(s) = (1+\beta)bs^{\beta}\exp(-bs^{1+\beta}), \tag{9}$$

with the parameter $\beta$ =1.0 and $b = (\Gamma[(2+\beta)/(1+\beta)]/D)^{1+\beta}$, $D$ is the average level spacing. Note that for the Poisson distribution the Brody parameter is equal zero.

If the QD shape represents a figure of rotation (cylindrical, ellipsoidal and others) then the 3D Schrödinger equation is separable. In cylindrical coordinates the wave function is written by the following form $\psi(\vec{r}) = \Phi(\rho, z)\exp(il\varphi)$, where $l = 0, \pm 1, \pm 3, \ldots$ is the electron orbital quantum number. The function $\Phi(\rho, z)$ is a solution of the two dimensional equation for cylindrical coordinates $\rho$ and $z$.

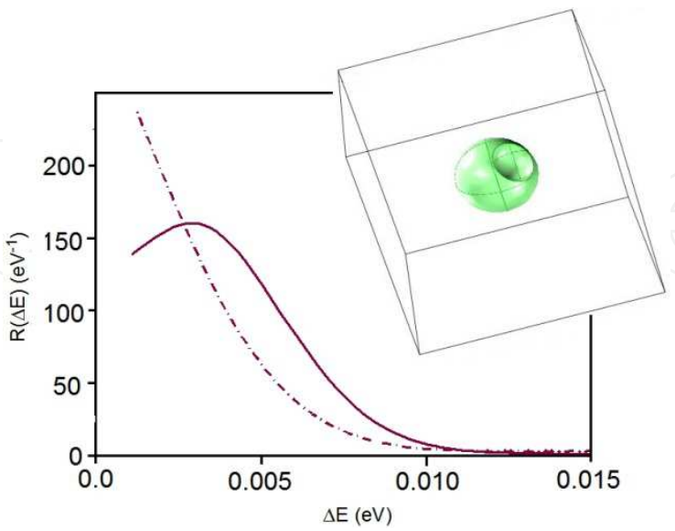


Fig. 17. Distribution functions for electron neighboring levels in $Si/SiO_2$ QD for spherical-like shape with cut. The Brody parameter $\beta$ =1.0. The geometry of this QD is shown in 3D. The QD diameter is 17 nm (inset).

Our results for the distribution function for the ellipsoidal shaped $Si/SiO_2$ QD are presented in Fig. 18a) (left). In the inset we show the cross section of the QD. The fitting of the calculated values for $R(\Delta E)$ gives the Poisson-like distribution. For the case of QD shape with the break of the ellipsoidal symmetry (Fig. 18b) (left)) by the cut below the major axis we obtained a non-Poisson distribution.

Fig. 18 (right) shows the that slightly deformed rhombus-like shape leads to the NNS with Brody parameter $\beta$ =1 (10). It is obvious why systems with different discrete symmetries reveal Poisson statistics: the different levels of the mixed symmetry classes of the spectrum of the quantum system are uncorrelated.

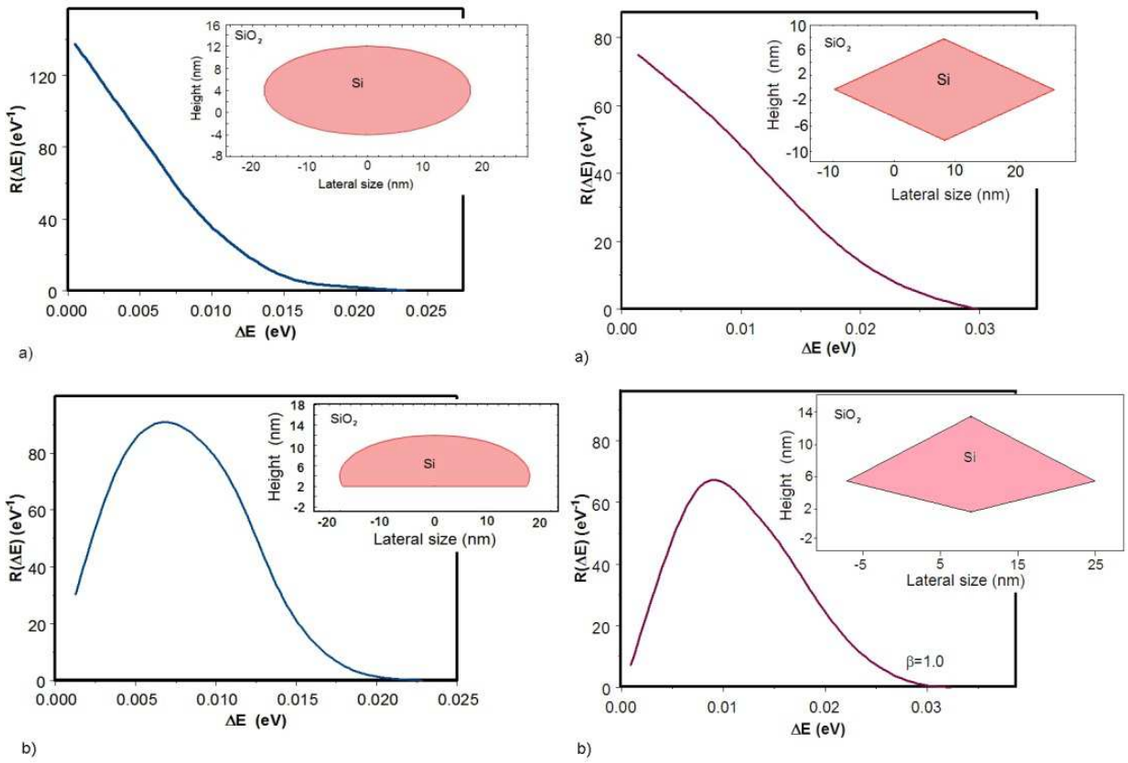


Fig. 18. (Left) Distribution functions for electron neighboring levels in $Si/SiO_2$ QD for different shapes: a) ellipsoidal shape, b) ellipsoidal like shape with cut. Brody parameter $\beta$ is defined to be equal 1.02 for the fitting of this distribution. The 3D QD shape has rotation symmetry. Cross section of the shapes is shown in the inset.
(Right). Violation of the shape Up-Down symmetry for $Si/SiO_2$ QD. Distribution functions for electron neighboring levels in $Si/SiO_2$ QD for different shapes: a) with rhombus cross section, b) with slightly deformed rhombus cross section. The 3D QD shape has rotation symmetry. The Brody parameter $\beta$ for the curve fitting this distribution is shown. Cross section of the shapes is shown in the inset.

In Schrödinger equation (7) in the asymptotical region of $\rho$ one can neglect the two terms $\frac{1}{\rho}\frac{\partial}{\partial\rho}$ and $-\frac{l^2}{\rho^2}$ of this equation. The solution of Eq. (7) can demonstrate the same

properties of the solution of the Schrödinger equation for 2D planar problem in Cartesian coordinates with the same geometry of QD shape in the asymptotical region. We illustrate this fact by Fig. 19. In this figure the violation of the shape Up-Down symmetry for 2D $Si/SiO_2$ QD is clarified. We compare the distribution functions for QD with "regular" semi-ellipsoidal shape (dashed curve in Fig. 19 a) and for QD with the semi-ellipsoidal shape having the cut (solid curve) as it are shown in Fig. 19 b). In the first case there is Up-Down symmetry of the QD shape. Corresponding distribution functions is Poissonian type. In second case the symmetry is broken by cut. The level statistics become non Poissonian. We have qualitative the same situation as for QD having rotation symmetry in 3D, presented in Fig. 18 (left) for the QD shape with rotation symmetry in cylindrical coordinates. The relation between the symmetry of QD shape and NNS is presented by Fig. 20 where we show the results of calculation of NNS for the 2D InAs/GaAs quantum well (QW). The two types of the statistics are presented in Fig. 20(left). The Poisonian distribution corresponds to shapes shown in Fig. 20 (b)-(d)(left) with different type of symmetry. The non-Poissonian distribution has been obtained for the QW shape with cut (a) which violated symmetry of initial shape (b), which is square having left-right symmetry, up-down symmetry, and diagonal reflection symmetry. The shape of the Fig. 20c) has only diagonal reflection symmetry. In Fig. 20d) the left-right symmetry of the shape exists only. The electron wave function of the high excited state, which contour plot is shown with the shape contour in Fig. 20(left), reflects the symmetry properties of the shapes.

Concluding, we can note that, obviously, the topological equivalent transformations of QD shape (keeping at least one discrete symmetry) do not lead to the non Poissonian distribution of the levels.

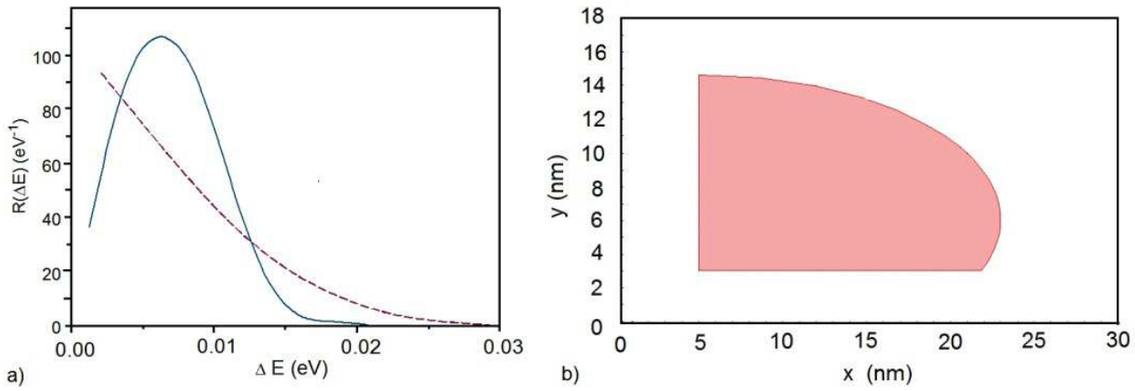


Fig. 19. Violation of the shape Up-Down symmetry for two dimensional $Si/SiO_2$ QD. a) Distribution functions for electron neighboring levels for the "regular" semi-ellipsoidal shape (dashed curve), for the semi-ellipsoidal shape with the cut (solid curve). b) The shape of the QD with cut (in Cartesian coordinates).

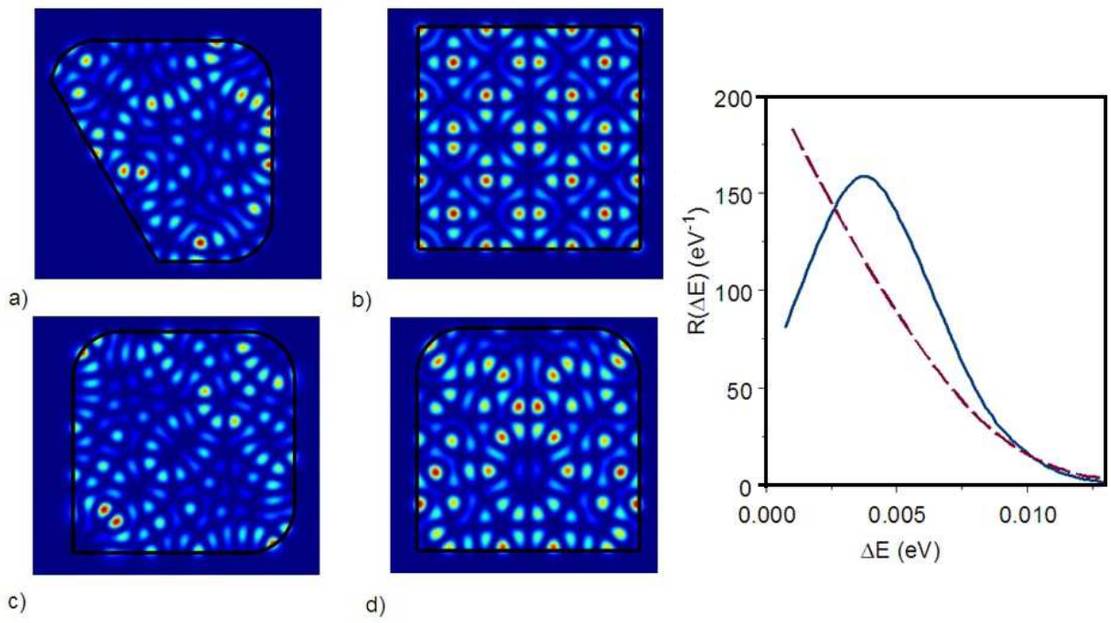


Fig. 20. Shape of the 2D InAs/GaAs quantum dots (Left). The black curves mean the perimeters. The electron wave function contour plots of the excited state (with energy about 0.5 eV are shown). The corresponding types of the level statistics are shown (Right). The shape a) leads to non-Poissonian statistics (solid curve). The shapes b)-d) result to the Poissonian statistics (dashed curve).

## 4. Double quantum dots and rings: New features

### 4.1 Disappearance of quantum chaos in coupled chaotic quantum dots

In the previous section, we investigated the NNS for various shape of the single quantum dots (SQD) in the regime of the weak confinement when the number of the levels allows to use quite sufficient statistics. Referring for details to (Filikhin et al., 2010), we briefly sum up the main conclusions of previous section: SQDs with at least one mirror (or rotation) symmetry have a Poisson type NNS whereas a violation of this symmetry leads to the Quantum Chaos type NNS.

In this section we study quantum chaotic properties of the double QD (DQD). By QD here we mean the three dimensional (3D) confined quantum object, as well its 2D analogue - quantum well (QW). In three dimensional case we use an assumption of the rotational symmetry of QD shape. The presented effective approach is in good agreement with the experimental data and previous calculations in the strong confinement regime (Filikhin et al., 2010). Here, in the regime of weak confinement, as in (Filikhin et al., 2010), we also do not consider Coulomb interaction between electron and hole: Coulomb effects are weak when the barrier between dots is thin leading to the strong interdot tunneling and dot sizes are large enough. In these circumstances, studied in detail in (Bryant, 1993) (see also for short review a monograph (Bimberg et al., 1999), one may justify disregard of the Coulomb effects. The physical effect, we are looking for, has place just for thin barriers; to have sufficient level statistics, we need large enough QDs (≥100 nm for InAs/GaAs QW).

Thus, we consider tunnel coupled two QDs with substrate between, which serves as barrier with electronic properties distinct from QD. Boundary conditions for the single electron Schrödinger equation are standard. We take into account the mass asymmetry inside as well outside of QDs (Filikhin et al., 2010). To avoid the complications connected with spin-orbit coupling, *s*-levels of electron are only considered in the following. We would like to remind that the selection of levels with the same quantum numbers is requisite for study of NNS and other types of level statistics.

Whereas at the large distances between dots each dot is independent and electron levels are twofold degenerate, expressing the fact that electron can be found either in one or in the other isolated dot, at the smaller inter-dot distances the single electron wave function begins to delocalize and extends to the whole DQD system. Each twofold degenerated level of the SQD splits by two, difference of energies is determined by the overlap, shift and transfer integrals (Bastard, 1990). Actually, due to the electron spin, there is fourfold degeneracy, however that does not change our results and below we consider electron as spinless. Note that the distance of removing degeneracy is different for different electron levels. This distance is larger for levels with higher energy measured relative to the bottom quantum well (see Fig. 23 below). By the proper choice of materials of dots and substrate one can amplify the "penetration" effects of the wave function.

Below we display some of our results for semiconductor DQDs. The band gap models are given in (Filikhin et al., 2010). Fig. 21 shows distribution function for two $Si/SiO_2$ QDs of the shape of the 3D ellipsoids with a cut below the major axis. Isolated QD of this shape, as we saw in the previous section, is strongly chaotic. It means that distribution function of this QD can be well fitted by Brody formula with the parameter which is close to unity (Filikhin et al, 2010). We see that the corresponding up-down mirror symmetric DQD shows Poisson-like NNS. Note that these statistics data involved 300 confined electron levels, which filled the quantum well from bottom to upper edges. We considered the electron levels with the orbital momentum $l$=0, as was mentioned above. The orbital momentum of electron can be defined due to rotational symmetry of the QD shape.

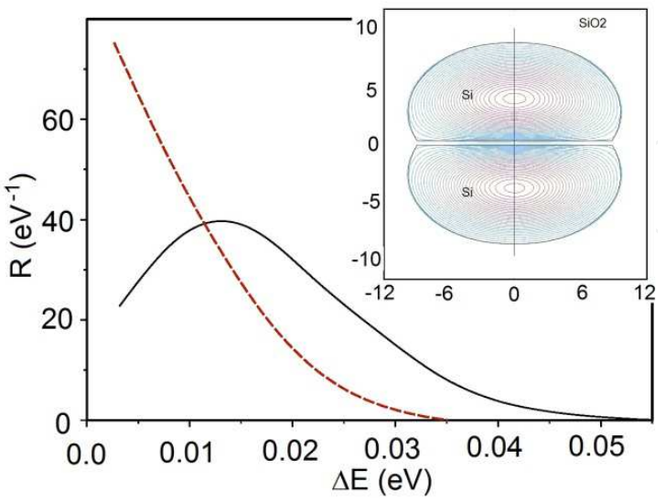


Fig. 21. The electron wave function of the ground state is shown by the contour plot. (The lower figure) Distribution functions for energy differences of the electron neighbori between QDs in InAs/GaAs DQD.

In Fig. 22, SQD (2D quantum well) without both type of symmetry reveals level repulsion, two tunnel coupled dots show the level attraction. From the mirror symmetry point of view, the chaotic character of such single object is due to the lack of the R-L and up-down mirror symmetries. The symmetry requirements in this case, for the coupled dots are less restrictive: presence of one of the mirror symmetry types is sufficient for the absence of quantum chaos.

Dependence NNS on the interdot distance shows a gradual transition to the regular behaviour with intermediate situation when Poisson-like behavior coexists with chaotic one: they combine but the level attraction is not precisely Poisson-like. Further decreasing distance restores usual Poisson character (see Fig. 22). Fig. 23 shows how the degeneracy gradually disappears with the distance $b$ between QDs in InAs/GaAs DQD.

Finally, we would like to show the disappearance of the Quantum Chaos when chaotic QW is involved in the "butterfly double dot" (Whitney, 2009) giving huge conductance peak in the semi-classical approach. Fig. 24 shows the NNS for chaotic single QW of (Whitney, 2009) by dashed line. Mirror (up-down and L-R) symmetry is violated. The NNS for an L-R mirror symmetric DQW is displayed by solid line in Fig. 24. It is clear that Quantum Chaos disappears.

We conjecture that the above mentioned peak in conductance of (Whitney, 2009) and observed here a disappearance of Quantum Chaos in the same array are the expression of the two faces of the Quantum Mechanics with its semi-classics and genuine quantum problem of the energy levels of the confined objects, despite the different scales (what seems quite natural) in these two phenomena (several micrometers and 10–100 nm, wide barrier in the first case and narrow one in the second). We have to emphasize here that the transport properties are mainly the problem of the wave function whereas the NNS is mainly the problem of eigenvalues. Similar phenomena are expected for the several properly arranged coupled multiple QDs and QD superlattices. In the last case, having in mind, for simplicity, a linear array, arranging the tunnel coupling between QDs strong enough, we will have wide mini-bands containing sufficient amount of energy levels and the gap between successive mini-bands will be narrow. Since the levels in the different mini-bands are uncorrelated, the overall NNS will be Poissonian independently of the chaotic properties of single QD. We would like to remark also that our results have place for 3D as well as for 2D quantum objects. It is important to notice that the effect of reduction of the chaos in a system of DQD could appear for interdot distances larger than considered, for instance in figure 22, if an external electrical field is applied. By properly designed bias the electric field will amplify wave function "penetration" effectively reducing a barrier between QDs.

Thus, we have shown that the tunnel coupled chaotic QDs in the mirror symmetric arrangement have no quantum chaotic properties, NNS shows energy level attraction as should to be for regular, non-chaotic systems. These results are confronted with the huge conductance peak found by the semi-classical method in (Whitney, 2009). We think that our results have more general applicability for other confined quantum objects, not only for the quantum nanostructures, and may be technologically interesting. Concerning the last issue, problem is what easer: try to achieve regular, symmetric shape of SQDs, or, not paying attention to their irregular, chaotic shape arrange more or less symmetric mutual location (Ponomarenko et al., 2008).

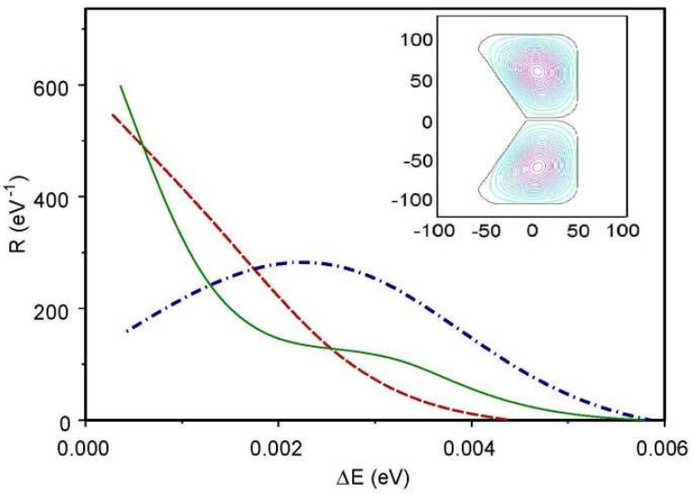


Fig. 22. Distribution functions for energy differences of the electron neighboring levels in the 2D InAs/GaAs DQW calculated for various distances $b$ between QWs. Dashed (solid) line corresponds to $b$ =4 nm ($b$ =2 nm). Distribution functions of single QW is also shown by the dot-dashed line. The DQW shape is shown in inset (sizes are in nm).

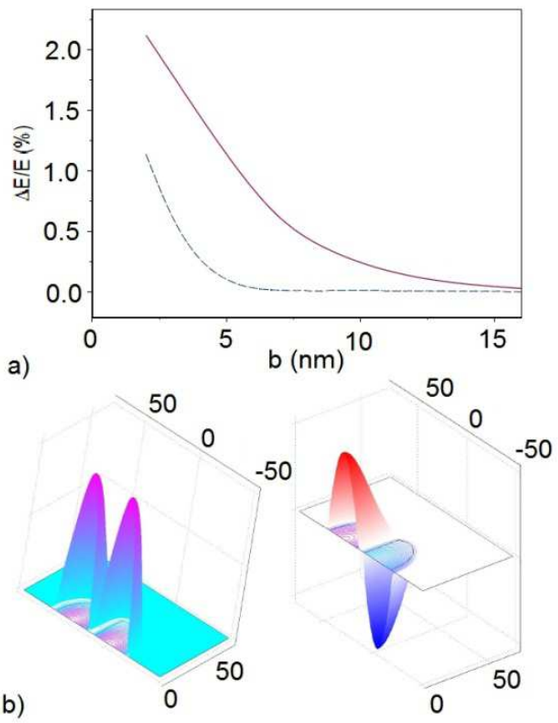


Fig. 23. (The upper figure) Doublet splitting $\Delta E$ of single electron levels dependence on the distance $b$ between QDs in InAs/GaAs DQD. The ground state ($E$ =0.23 eV) level splitting is $\Delta E$ expressed by dashed line. The solid line corresponds to doublet splitting of a level which is close to upper edge of the quantum well ($E$ =0.56 eV). The shape of DQD is the same as in Fig. 21 (The lower figure). The electron wave functions of the doublet state: the ground state (left) and first excited state (right), are shown.

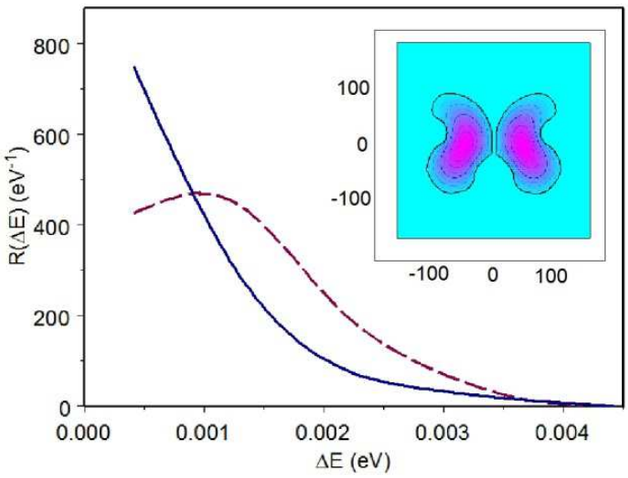


Fig. 24. Distribution functions for electron neighboring levels in InAs/GaAs single QW (dashed line) and DQW (solid line). Shape of DQW is shown in the inset. The electron wave function of the ground state is shown by the contour plot in the inset. Data of the statistics include 200 first electron levels.

### 4.2 Electron transfer between pair of concentric quantum rings in magnetic field

Quantum rings are remarkable meso- and nanostructures due to their non-simply connected topology and attracted much attention last decade. This interest supported essentially by the progress in the fabrication of the structures with wide range of geometries including single and double rings. This interest rose tremendously in the connection to the problem of the persistent current in mesoscopic rings (Buttiker et al., 1983) Transition from meso - to nano - scale makes more favorable the coherence conditions and permits to reduce the problem to the few or even to single electron.

Application of the transverse magnetic field $B$ leads to the novel effects: Whereas the quantum dots (QDs) of the corresponding shape (circular for two dimensional (2D), cylindrical or spherical for 3D ) has degeneracy in the radial $n$ and orbital $l$ quantum numbers, QR due to the double connectedness in the absence of the magnetic field $B$ has degeneracy only in $l$, and the nonzero $B$ lifts the degeneracy in $l$, thus making possible the energy level crossing at some value of $B$, potentially providing the single electron transition from one state to the another.

Use the configurations with double concentric QR (DCQR) reveals a new pattern: one can observe the transition between different rings in the analogy with atomic phenomena. For the DCQR, the 3D treatment is especially important when one includes the inter-ring coupling due to the tunneling. The dependence on the geometries of the rings (size, shape and etc.) becomes essential.

We investigate the electron wave function localization in double concentric quantum rings (DCQRs) when a perpendicular magnetic field is applied. In weakly coupled DCQRs can be arisen the situation, when the single electron energy levels associated with different rings may be crossed. To avoid degeneracy, the anti-crossing of these levels has a place. In this DCQR the electron spatial transition between the rings occurs due to the electron level anti-crossing. The anti-crossing of the levels with different radial quantum numbers (and equal

orbital quantum numbers) provides the conditions when the electron tunneling between rings becomes possible. To study electronic structure of the semiconductor DCQR, the single sub-band effective mass approach with energy dependence was used (see section 2 of this Chapter). Realistic 3D geometry relevant to the experimental DCQR fabrication was employed taken from (Kuroda et al., 2005; Mano et al., 2005). The GaAs QRs and DQRs rings, embedded into the $Al_{0.3}Ga_{0.7}As$ substrate, are considered (Filikhin, et al., 2011). The strain effect between the QR and the substrate materials was ignored here because the lattice mismatch between the rings and the substrate is small. Due to the non-parabolic effect taken into account by energy dependence effective mass of electron in QR, the effective mass of the electron ground state is calculated to be the value of $0.074\, m_0$ that is larger than the bulk value of $0.067\, m_0$ . For the excited states, the effective mass will increase to the bulk value of the $Al_{0.3}Ga_{0.7}As$ substrate. Details of this calculation one can find in (Filikhin, et al. 2011).

Electron transfer in the DCQR considered is induced by external factor like a magnetic or electric fields. Probability of this transfer strongly depends on the geometry of DCQR. The geometry has to allow the existing the weakly coupled electron states. To explain it, we note that DCQR can be described as a system of double quantum well. It means that there is duplication of two sub-bands of energy spectrum (see (Manasreh, 2005) for instance) relative the one for single quantum object. In the case of non-interacting wells (no electron tunneling between wells) the each sub-band is related with left or right quantum well. The wave function of the electron is localized in the left or right quantum well. When the tunneling is possible (strong coupling state of the system), the wave function is spread out over whole volume of the system. In a magnetic field, it is allowed an intermediate situation (weak coupled states) when the tunneling is possible due to anti-crossing of the levels. Anti-crossing, of course, is consequence of the impossibility to cross of levels with the same space symmetry (von Neumann & Wigner, 1929; Landau & Lifshitz, 1977).

There is a problem of notation for states for DCQR. If we consider single QR (SQR) then for each value of the orbital quantum number $|l| = 0, 1, 2...$ in Eq. (7) we can definite radial quantum number $n$ =1,2,3,… corresponding to the numbers of the eigenvalues of the problem (7) in order of increasing. One can organize the spectrum by sub-bands defined by different $n$ . When we consider the weakly coupled DCQR, in contrast of SQR, the number of these sub-bands is doubled due to the splitting the spectrum of double quantum object (Bastard, 1990). Electron in the weakly coupled DCQR can be localized in the inner or outer ring. In principle, in this two ring problem one should introduce a pair of separate sets of quantum numbers $(n_i, l)$ where index $i$ =1,2 denoted the rings where electron is localized. However, it is more convenient, due to the symmetry of the problem, to have one pair $(n, l)$ numbers ascribed to both rings (inner or outer), in other words, we use a set of quantum numbers $(n, l), p$ where $p$ is dichotomic parameter attributed to the electron localization ("inner" or "outer" ).

Since we are interested here in the electron transition between rings and, as we will see below, this transition can occur due to the electron levels anti-crossing followed a tunneling, we concentrate on the changing of the quantum numbers $n$ . The orbital quantum numbers must be equal providing the anti-crossing of the levels with the same symmetry (see Landau & Lifshitz, 1977). Thus, the anti-crossing is accompanied by changing the quantum numbers $n$ and $p$ of the $(n, l), p$ set.

Strongly localized states exist in the DCQR with the geometry motivated by the fabricated DCQR in (Kuroda et al., 2005; Mano et al., 2005). The wave functions of the two $s$-states of the single electron with $n$=1,2 are shown in Fig. 25, where the electron state $n$=1 is localized in outer ring, and the electron state $n$=2 is localized in inner ring. Moreover all states of the sub-bands with $n$=1,2, and $|l|$=1,2,3… are well localized in the DCQR. The electron localization is outer ring for $n$=1, $|l|$=0,1,2,…, and inner ring for $n$=2, $|l|$=0,1,2….

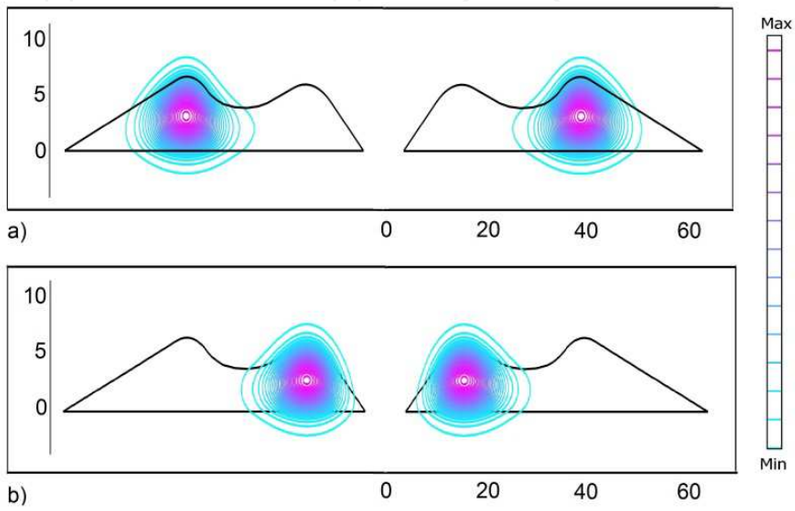


Fig. 25. The squares of wave functions for the a) $(1,0)$ ,outer ( $E=0.072$ eV) and b) $(2,0)$ ,inner ( $E=0.080$ eV) states are shown by contour plots. The contour of the DCQR cross-section is given. The sizes are in nm.

The difference of properties of the two sub-bands can be explained by competition of two terms of the Hamiltonian of Eq. (7) and geometry factor. The first term includes first derivative of wave function over $\rho$ in kinetic energy; the second is the centrifugal term. For $|l|\neq 0$ the centrifugal force pushes the electron into outer ring. One can see that the density of the levels is higher in the outer ring. Obviously, the geometry plays a role also. In particular, one can regulate density of levels of the rings by changing a ratio of the lateral sizes of the rings.

Summarizing, one can say that for $B$=0 the well separated states are only the states $(1,l),p$ and $(2,l),p$ . Thus, used notation is proper only for these states. The wave functions of the rest states $(n>2,l)$ are distributed between inner and outer rings. These states are strongly coupled states.

Crossing of electron levels in the magnetic field $B$ are presented in Fig. 26 There are crossings of the levels without electron transfer between the rings. This situation is like when we have crossing levels of two independent rings. There are two crossings when the orbital quantum number of the lower state is changed due to the Aharonov-Bohm effect. It occurs at about 0.42 T and 2.5 T. There are two anti-crossings: the first is at 4.8 T, another is at 5.2 T. These anti-crossings are for the states with different $n$ ; the first are states (1,0) and (2,0) and the second are states (1,-1) and (2,-1). In these anti-crossings the possibility for electron tunneling between rings are realized. In Fig. 27 we show how the root mean square (rms) of the electron radius is changed due to the tunneling at anti-crossing. One can see

from Fig. 26 that the electron transition between rings is only possible when the anti-crossed levels have different radial quantum numbers and equal orbital quantum numbers, in accordance of (von Neuman & Vigner, 1929).

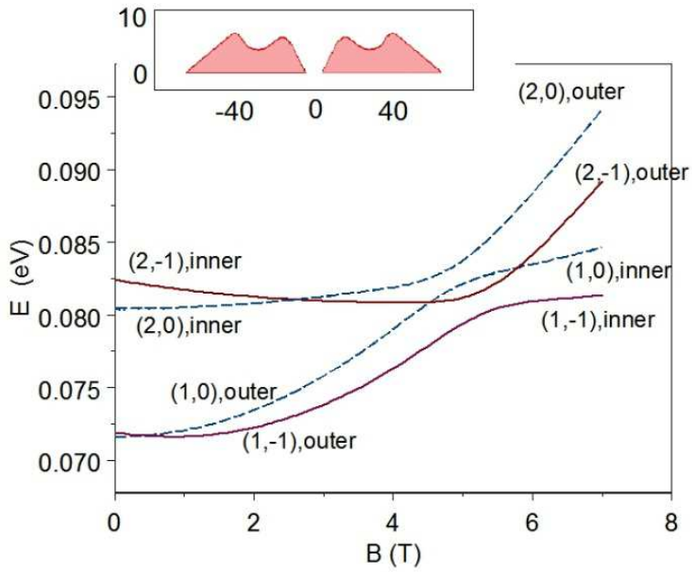


Fig. 26. Single electron energies of DCQR as a function of magnetic field magnitude $B$. Notation for the curves: the double dashed (solid) lines mean states with $l$=0 ($l$=-1) with $n$=1,2. The quantum numbers of the states and positions of the electron in DCQR are shown. The cross section of the DCQR is given in the inset.

Transformation of the profile of the electron wave function during the process of anti-crossing with increasing $B$ is given in Fig. 28. The electron state (1,-1), outer is considered as "initial" state of an electron ($B$=0). The electron is localized in outer ring. Rms radius is calculated to be $R$=39.6 nm. For $B$=5.2 T the second state is the tunneling state corresponding to the anti-crossing with the state (0,-1). The wave function is spreaded out in both rings with $R$=32.7 nm. The parameter $p$ has no definite value for this state. The "final" state is considered at $B$=7 T. In this state the electron was localized in inner ring with $R$=17.6 nm. Consequently connecting these three states of the electron, we come to an electron trapping, when the electron of outer ring ("initial" state) is transferred to the inner ring ("final" state). The transfer process is governed by the magnetic field.

Note that the energy gap between anti-crossed levels which one can see in Fig. 26 can be explained by the general theory for double interacting quantum well (Bastard, 1990). The value of the gap depends on separation distance between the rings, governed by the overlapping wave functions corresponding to the each ring, and their spatial spread which mainly depends on radial quantum number of the states (Filikhin et al., 2011).

Other interesting quantum system is one representing QR with QD located in center of QR. The cross section of such heterostructure ($GaAs/Al_{0.3}Ga_{0.7}As$) is shown in Fig. 29a. In Fig. 29b we present the results of calculations for electron energies of the (1,0) and (3,0) states in the magnetic field $B$ (Filikhin et al., 2011). Once more we can the level anti-crossing (for about of 12.5 T). This anti-crossing is accompanied by exchange of electron localization

between the QD and the QR. In other words if initial state (for $B$ <12.5 T) of electron was the state (1,0),outer, then the "final" state (for $B$ >12.5 T) will be (1,0),inner. It can be considered as one of possibilities for trapping of electron in QD.

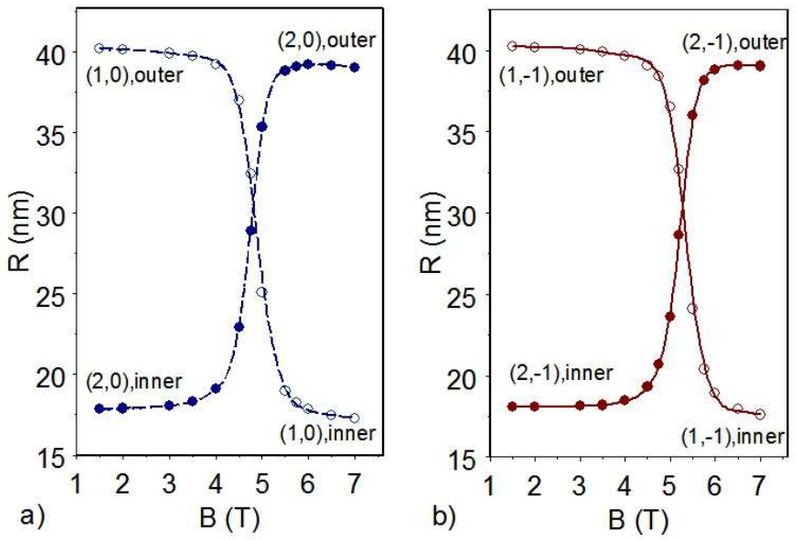


Fig. 27. Rms radius of an electron in DCQR as a function of magnetic field for the states a) $((n=1,2), l=0)$ and b) $((n=1,2), l=-1)$ near point of the anti-crossing. The calculated values are shown by solid and open circles. The dashed (solid) line, associated with states of $l=0$ ($l=-1$), fits the calculated points.

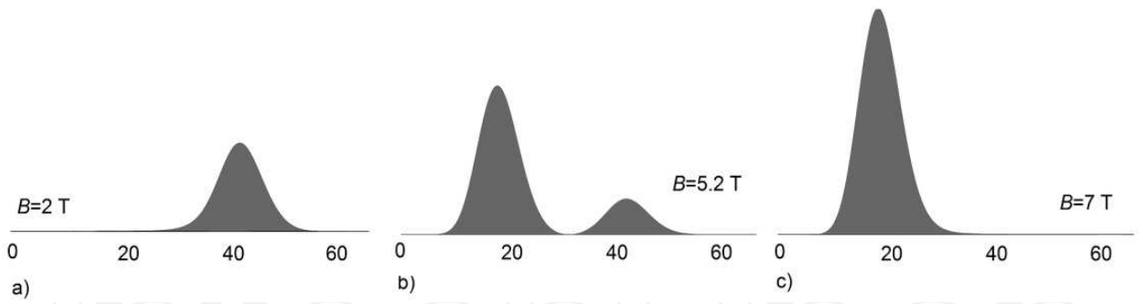


Fig. 28. Profiles of the normalized square wave function of electron in the states a) $(1,-1)$ ,outer; b) $(1,-1)$ ,n/a and c) $(1,-1)$ ,inner for different magnetic field $B$. The a) is the "initial" state ($B$ =0) with $R$ =39.6 nm, the b) is the state of electron transfer ($B$ =5.2 T) with $R$ =32.7 nm, the c) is the "final" state ($B$ =7 T) with $R$ =17.6 nm. The radial coordinate $\rho$ is given in nm (see Fig. 26 for the DCQR cross section).

One can see from Fig. 29b that the energy of the dot-localized state grows more slowly than the envelope ring-localized state. At the enough large $B$ the dot-localized state becomes the ground state (Szafran et al., 2004). In other words, when the Landau orbit of electron becomes smaller then dot size, electron can enter the dot without an extra increase of kinetic energy.

Concluding, we made visible main properties of this weakly coupled DCQD established by several level anti-crossings that occurred for the states with different radial quantum number $n$ ($n$ =1,2) and equal orbital quantum number $l$. One may conclude that the fate of

the single electron in DCQRs is governed by the structure of the energy levels with their crossing and anti-crossing and is changing with magnetic field. The above described behavior is the result of the nontrivial excitation characteristic of the DCQRs. Effect of the trapping of electron in inner QR (or QD) of DCQR may be interesting from the point of view of quantum computing.

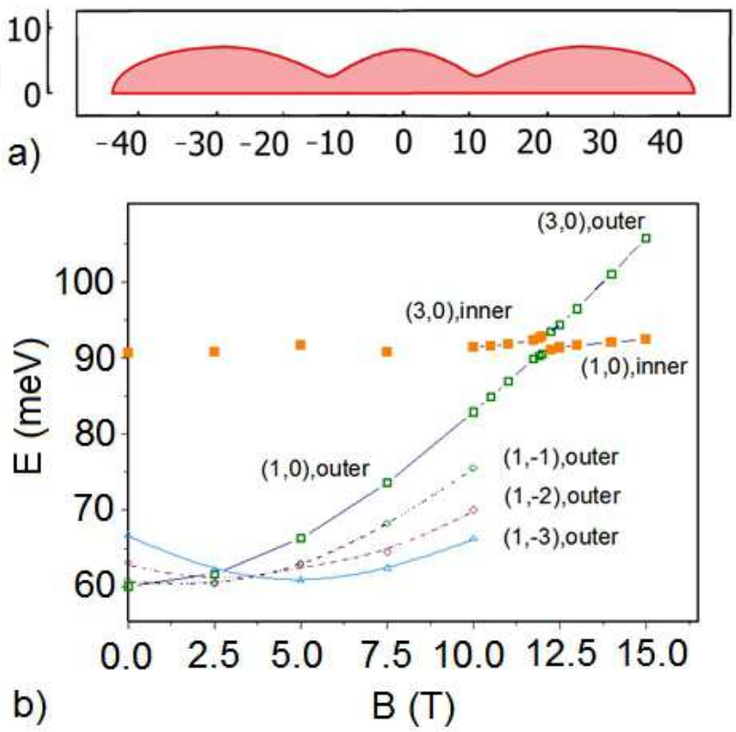


Fig. 29. a) Cross section of the QR with QD system. Sizes are given in nm. b) Energies of the (1,0) and (3,0) states in the magnetic field $B$ for the QR with QD system. The open symbols show that the electron is localized in the ring. The solid squares show that the electron localized in QD.

## 5. Acknowledgment

This work is supported by NSF CREST award; HRD-0833184 and NASA award NNX09AV07A

## 6 References

Aharonov Y. & Bohm, D. (1959). Significance of Electromagnetic Potentials in the Quantum Theory, *Physical Review,* Vol. 115, Issue 3, (1959), pp. 485–491

Alferov, Zh.I. (1998).The history and future of semiconductor heterostructures, *Semiconductors*, Vol. 32, No. 1 (January 1998), pp. 1-14, ISSN 1063-7826 (Print); 1090-6479 (Online)

Anderson P.W. ; Thouless D.J.; Abrahams, E.; Fisher, D. S. (1980). New method for a scaling theory of localization. *Physical Review B*, Vol. 22, Issue 8, (1980), pp. 3519–3526, ISSN 1550-235x (online), 1098-0121 (print)

Aronov A.G. & Sharvin, Yu.V. (1987). Magnetic flux effects in disordered conductors, *Review Modern Physics*. Vol. 59, (1987), pp. 755–779, ISSN 1539-0756 (online), 0034-6861 (print)

Baranger, H.U. & Stone, A.D. (1989). Quenching of the Hall resistance in ballistic microstructures: A collimation effect, *Physical Review Letters*, Vol. 63, (1989), pp. 414–417, ISSN 1079-7114 (online) 0031-9007 (print)

Baranger, H.U.; DiVincenzo, D.P.; Jalabert R.A. & Stone, A.D. (1991). Classical and quantum ballistic-transport anomalies in micro-junctions, *Physical Review B*, Vol. 44, Issue 19, (1991), pp. 10637–10675, ISSN 1550-235x (online), 1098-0121 (print)

Bastard, G. (1990).*Wave Mechanics applied to Semiconductor Heterostructures,* John Wiley and Sons Inc. (Jan 01, 1990), p. 357, ISBN 0-471-21708-1, New York, NY (USA)

Beenakker, C.W.J. & van Houten, H. (1991). *Solid State Physics: Advances in Research and Applications*, Ed. H. Ehrenreich and D. Turnbull, Academic Press (April 2, 1991), Vol. 44, (1991), p.1-454, ISBN-10: 0126060444, N-Y, USA

BenDaniel D. J. & Duke C. B. (1966). Space-Charge Effects on Electron Tunneling, *Physical Review*, Vol. 152, Issue 2, (1966), pp. 683–692,

Betcke, M.M. & Voss, H. (2011). Analysis and efficient solution of stationary Schrödinger equation governing electronic states of quantum dots and rings in magnetic field, https://www.mat.tu-harburg.de/ins/forschung/rep/rep143.pdf; to appear in CiCT (2011)

Bimberg, D.; Grundmann, M.; Ledentsov, N.N. (1999). *Quantum Dot Heterostructure*, John Wiley and Sons Inc. (1999), ISBN 0-471-97388-2, Chichester, England

Bloch, F. (1928). Über die Quantenmechanik der Elektronen in Kristallgittern, *Zeitschrift fur Physik*, Vol. 52, Issue 7-8, (1928), pp. 555–600, ISSN 0939-7922 (Print), 1431-5831 (Online)

Brody, T. A.; Flores, J.; French, J. B.; Mello, P. A.; Pandey, A.; Wong, S. S. M. (1981). Random-matrix physics: spectrum and strength fluctuations, *Reviews of Modern Physics*, Vol. 53, Issue 3, (1981) pp. 385–479, ISSN 1539-0756 (online), 0034-6861 (print).

Bryant, G.W (1993). Electrons in coupled vertical quantum dots: Interdot tunneling and Coulomb correlation, *Physical Review B*, Vol. 48, Issue 11, (1993), pp. 8024–8034, ISSN 1550-235x (online), 1098-0121 (print)

Bryant, G.W. (1992). Indirect-to-direct crossover of laterally confined excitons in coupled quantum wells. *Physical Review B,* Vol. 46, Issue 3, (1992), pp. 1893–1896, ISSN 1550-235x (online), 1098-0121 (print)

Buttiker, M. , Imry Y. & Landauer, R. (1983). Josephson behavior in small normal one-dimensional rings, *Physics Letters A*, Vol. 96, Issue 7, 1(8 July 1983), pp. 365-367, ISSN 0375-9601

Califano, M. & Harrison, P. (2000). Presentation and experimental validation of a single-band, constant-potential model for self-assembled InAs/GaAs quantum dots, *Physical Review B*, Vol. 61, (2000), pp. 10959–10965, ISSN 1550-235x (online), 1098-0121 (print)

Chakraborty, T. & Pietiläinen, P. (1994). Electron-electron interaction and the persistent current in a quantum ring. *Physical Review B*, Vol. 50, pp. 8460–8468, ISSN 1550-235x (online), 1098-0121 (print)

Duque, C.A.; Porras-Montenegro, N.; Barticevic, Z.; Pachecoc, M.; Oliveira, L.E. (2005). Electron-hole transitions in self-assembled InAs/GaAs quantum dots: Effects of

applied magnetic fields and hydrostatic pressure, *Microelectronics Journal* 36, (2005), pp. 231-233, ISSN 0026-2692

Emperador, A.; Pi, M.; Barranco, M.; Lorke, A. (2000). Far-infrared spectroscopy of nanoscopic InAs rings, *Physical Review B,* Vol. 62, (2000), pp. 4573. 4573–4577, ISSN 1550-235x (online), 1098-0121 (print)

Filikhin I, E. Deyneka & Vlahovic, B (2007a) Numerical modeling of experimentally fabricated InAs/GaAs quantum rings, *Molecular Simulation*, Vol. 33, Issue 7, (2007), pp. 589-592, ISSN 0892-7022 (Print), 1029-0435 (Online)

Filikhin, I.; Deyneka, E. & Vlahovic, B. (2006a). Non parabolic model for InAs/GaAs quantum dot capacitance spectroscopy, *Solid State Communications* 140, (2006), pp. 483–486, ISSN 0038-1098

Filikhin, I.; Deyneka, E.; Melikyan, H. & Vlahovic, B. (2005). Electron States of Semiconductor Quantum Ring Electron States of Semiconductor Quantum Ring with Geometry and Size Variations, *Journal Molecular Simulation*, Vol. 31, (2005), pp. 779-782, Print ISSN 0892-7022, Online ISSN 1029-0435

Filikhin, I.; Matinyan, S.; Nimmo, J. & Vlahovic, B. (2011). Electron Transfer between Weakly Coupled Concentric Quantum Rings, *Physica E: Low-dimensional Systems and Nanostructures,* Vol. 43, No. 9, (July 2011), pp. 1669-1676, ISSN: 1386-9477

Filikhin, I.; S.G. Matinyan, S.G.; Schmid, B.K. & Vlahovic, B. (2010). Electronic and level statistics properties of Si/SiO2 quantum dots, *Physica E: Low-dimensional Systems and Nanostructures*, Vol. 42, Issue 7, (May 2010), pp. 1979-1983, ISSN: 1386-9477.

Filikhin, I.; Suslov, V. M.; Wu, M. & Vlahovic, B. (2008). Effective approach for strained InAs/GaAs quantum structures. *Physica E: Low-dimensional Systems and Nanostructures*, Vol. 40, (2008), pp. 715–723, ISSN: 1386-9477

Filikhin, I.; Suslov, V.M. & Vlahovic, B. (2006). Modeling of InAs/GaAs quantum ring capacitance spectroscopy in the nonparabolic approximation, *Physical Review B*, Vol. 73, (2006), pp. 205332-205336, ISSN 1550-235x (online), 1098-0121 (print)

Filikhin, I.; Suslov, V.M. & Vlahovic, B. (2009) InGaAs/GaAs quantum dots within an effective approach, *Physica E: Low-dimensional Systems and Nanostructures*, Vol. 41, (2009), pp. 1358–1363, ISSN: 1386-9477

Filikhin, I.N., Deyneka, E. & Vlahovic, B. (2004). Energy dependent effective mass model of InAs/GaAs quantum ring, *Modelling and Simulation in Materials Science and Engineering*, Vol. 12, (2004), pp. 1121-1126, ISSN 0965-0393 (Print); ISSN 1361-651X (Online)

Filikhin, I; Suslov, V.M. & Vlahovic, B. (2011a). C-V Data and Geometry Parameters of Self-Assembled InAs/GaAs Quantum Rings, accepted for publication in *Journal of Computational and Theoretical Nanoscience* (2011), ISSN:1546-1955

Fu, H.; Wang, L.-W.; Zunger, A. (1998). Applicability of the k.p method to the electronic structure of quantum dots, *Physical Review B*, Vol. 57, (1998), pp. 9971, ISSN 1550-235x (online), 1098-0121 (print)

Gefen Y.; Imry, Y.; Azbel, M. Ya. (1984). Quantum Oscillations and the Aharonov-Bohm Effect for Parallel Resistors. *Physical Review Letters*, Vol. 52, Issue 2, (1984), pp. 129–132, ISSN 1079-7114 (online); 0031-9007 (print)

Harrison, P. (2005). *Quantum Wells, Wires And Dots: Theoretical And Computational Physics of Semiconductor Nanostructures,* Wiley-Interscience, (2005), pp. 1-497, ISBN:9780470010808

Kane, E.O. (1957), Band Structure of Indium Antimonide, *Journal of Physics and Chemistry of Solids*, Pergamon Press, Vol. 1, (1957), pp. 249-261, ISSN 0022-3697

Keldysh, L. V. (1962). *Soviet Physics Solid State,* Vol. 4, (1962), pp. 2265, ISSN: 0038-5654

Landau, L.D. & Lifschitz, E. M. *Quantum Mechanics (Non-Relativistic Theory)*, 3rd ed. Pergamon Press, (1977), ISBN 0080209408, Oxford, England

Landauer, R. (1970). Electrical resistance of disordered one-dimensional lattices, *Philosophical Magazine*, Vol. 21, Issue 172, (1970) pp. 863-867, ISSN 1478-6443

Lei, W.; Notthoff, C.; Lorke, A.; Reuter, D. & Wieck, A. D. (2010). Electronic structure of self-assembled InGaAs/GaAs quantum rings studied by capacitance-voltage spectroscopy, Applied Physics Letters, Vol. 96, (2010), pp. 033111-033114, Print: ISSN 0003-6951, Online: ISSN 1077-3118

Li, Bin & Peeters F. M. (2011). Tunable optical Aharonov-Bohm effect in a semiconductor quantum ring. *Physical Review B*, Vol. 83, (28 March 2011) pp. 115448-13, ISSN 1550-235x (online), 1098-0121 (print)

Li, S.S. & Xia, J.B. (2001). Electronic states of InAs/GaAs quantum ring, *Journal Applied Physics*, Vol. 89, (2001), pp. 3434-3438, Print: ISSN 0021-8979, Online: ISSN 1089-7550

Li, Y.; Voskoboynikov, O.; Lee, C.P. (2002). Computer simulation of electron energy states for three-dimensional InAs/GaAs semiconductor quantum ring, *Proceedings of the International Conference on Modeling and Simulating of Microsystems* (San Juan, Puerto Rico, USA), p. 543, Computational Publication, (2002), Cambridge

Lorke, A.; Luyken, R.J.; Govorov, A.O. & Kotthaus, J.P.; Garcia, J.M. & Petroff, P. M. (2000). Spectroscopy of Nanoscopic Semiconductor Rings, *Physical Review Letters*, Vol. 84, Issue 10, (March, 2000), pp. 2223–2226, ISSN 1079-7114 (online); 0031-9007 (print)

Manasreh, O. (2005). *Semiconductor Heterojunctions and Nanostructures (Nanoscience & Technology),* McGraw-Hill, (2005), p. 554, ISBN 0-07-145228-1, New York

Miller, B.T.; Hansen, W.;Manus, S.; Luyken, R.J.; Lorke, A; Kotthaus, J.P.; Huant, S.; Medeiros-Ribeiro, G; Petroff, P.M. (1997). Few-electron ground states of charge-tunable self-assembled quantum dots, *Physical Review B*, Vol. 56, (1997), pp. 6764–6769, ISSN 1550-235x (online), 1098-0121 (print)

Ponomarenko, L.A.; Schedin, F.; Katsnelson, M.I.; Yang, R.; Hill, E. W.; Novoselov K. S.; Geim A. K. (2008). Chaotic Dirac Billiard in Graphene Quantum Dots, *Science,* Vol. 320, No. 5874, (18 April 2008), pp. 356-358, ISSN 0036-8075 (print), 1095-9203 (online).

Rodt, S.; Schliwa, A.; Pötschke, K.; Guffarth, F.& Bimberg, D. (2005). Correlation of structural and few-particle properties of self-organized InAs/GaAs quantum dots, *Physical Review B*, Vol. 71, Issue 15, (2005), pp. 155325-155232, ISSN 1550-235x (online), 1098-0121 (print)

Schliwa, A.; Winkelnkemper, M. & Bimberg, D. Impact of size, shape, and composition on piezoelectric effects and electronic properties of In(Ga)As/GaAs quantum dots, *Physical Review B*, Vol. 76, (2007) pp. 205324-205341, ISSN 1550-235x (online), 1098-0121 (print)

Szafran, B. & Peeters, F.M. (2005). Few-electron eigenstates of concentric double quantum rings, *Physical Review B*, Vol. 72, (2005), pp. 155316-1555325, ISSN 1550-235x (online), 1098-0121 (print)

Szafran, B.; Peeters, F.M. & Bednarek, S. (2004). Exchange energy tuned by asymmetry in artificial molecules, *Physical Review B*, Vol. 70, Issue 20, (2004), pp. 205318-205323, ISSN 1550-235x (online), 1098-0121 (print).

T. Kuroda, T. Mano, T. Ochiai, S. Sanguinetti, K. Sakoda, G. Kido and N. Koguchi, (2005). Optical transitions in quantum ring complexes, *Physical Review B*, Vol. 72, Issue 20, (2005), pp. 205301–205309, ISSN 1550-235x (online), 1098-0121 (print)

T. Mano, T. Kuroda, S. Sanguinetti, T. Ochiai, T. Tateno, J. Kim, T. Noda, M. Kawabe, K. Sakoda, G. Kido, and N. Koguchi, (2005). Self-Assembly of Concentric Quantum Double Rings, *Nano Letters* , Vol. 5, No. 3, (2005), pp. 425–428, Print Edition ISSN 1530-6984, Web Edition ISSN 1530-6992

V. Neumann, J. & Wigner, E. (1929). Über das Verhalten von Eigenwerten bei adiabatischen Prozessen, *Physikalische Zeitschrift*, Vol. 30, (1929), pp. 467-468, OCLC Number 1762351

Voskoboynikov, O.; Li, Yiming; Lu, Hsiao-Mei; Shih, Cheng-Feng & Lee C.P. (2002). Energy states and magnetization in nanoscale quantum rings, *Physical Review B*, Vol. 66, (2002), pp. 155306-155312, ISSN 1550-235x (online), 1098-0121 (print).

Voss, H. (2005), Electron energy level calculation for a three dimensional quantum dot, Advances in Computational Methods in Sciences and Engineering 2005, selected papers from the *International Conference of Computational Methods in Sciences and Engineering 2005* (ICCMSE 2005) pp. 586 - 589, Leiden, The Netherlands; Editors: Theodore Simos and George Maroulis. ISBN 10 9067644412, 9067644439, 9067644447

Warburton R. J.; Miller, B. T.; Durr, C. S.; Bodefeld, C.; Karrai, K.; Kotthaus, J.P.; Medeiros-Ribeiro, G.; Petroff, P. M.; Huant, S. (1998). Coulomb interactions in small charge-tunable quantum dots: A simple model, *Physical Review B*, Vol. 58, Issue 24, (1998), pp. 16221–16231, ISSN 1550-235x (online), 1098-0121 (print)

Wetzel, C.; Winkler, R.; Drechsler M. & Meyer, B. K.;Rössler, U.; Scriba J. & Kotthaus, J. P.; Härle, V. & Scholz, F. (1996). Electron effective mass and nonparabolicity in Ga0.47In0.53As/InP quantum wells, *Physical Review B*, Vol. 53, (1996), pp. 1038–1041, ISSN 1550-235x (online), 1098-0121 (print)

Whitney, R.S.; Marconcini P. & Macucci, M. (2009a). Huge Conductance Peak Caused by Symmetry in Double Quantum Dots, *Physical Review Letters*, Vol. 102, (2009), pp. 186802-186806, ISSN 1079-7114 (online) 0031-9007 (print)

Whitney, R.S.; Schomerus, H. & Kopp, M. (2009). Semiclassical transport in nearly symmetric quantum dots. I. Symmetry breaking in the dot, *Physical Review E*, Vol. 80, Issue 5, (2009), 056209-056225, ISSN 1550-2376 (online), 1539-3755 (print)

Yu, P. & Cardona, M. (2005). *Fundamentals of Semiconductors: Physics and Materials Properties* (3rd ed.). Springer. Section 2.6, (2005), pp. 68, ISBN 3-540-25470-6

Zhao Q. & Mei, T. (2011). Analysis of electronic structures of quantum dots using meshless Fourier transform k·p method, *Journal of Applied Physics*, Vol. 109, Issue 6, (2011), pp. 063101-13, Print: ISSN 0021-8979, Online: ISSN 1089-7550

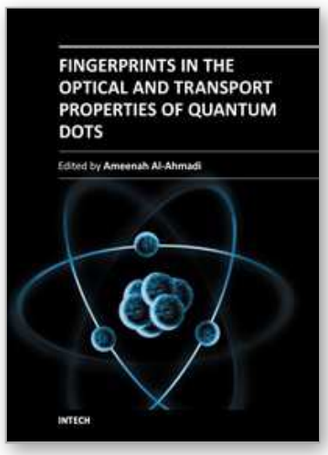


**Fingerprints in the Optical and Transport Properties of Quantum Dots**

Edited by Dr. Ameenah Al-Ahmadi

ISBN 978-953-51-0648-7
Hard cover, 468 pages
**Publisher** InTech
**Published online** 13, June, 2012
**Published in print edition** June, 2012

The book "Fingerprints in the optical and transport properties of quantum dots" provides novel and efficient methods for the calculation and investigating of the optical and transport properties of quantum dot systems. This book is divided into two sections. In section 1 includes ten chapters where novel optical properties are discussed. In section 2 involve eight chapters that investigate and model the most important effects of transport and electronics properties of quantum dot systems This is a collaborative book sharing and providing fundamental research such as the one conducted in Physics, Chemistry, Material Science, with a base text that could serve as a reference in research by presenting up-to-date research work on the field of quantum dot systems.

**How to reference**

In order to correctly reference this scholarly work, feel free to copy and paste the following:

I. Filikhin, S.G. Matinyan and B. Vlahovic (2012). Quantum Mechanics of Semiconductor Quantum Dots and Rings, Fingerprints in the Optical and Transport Properties of Quantum Dots, Dr. Ameenah Al-Ahmadi (Ed.), ISBN: 978-953-51-0648-7, InTech, Available from: http://www.intechopen.com/books/fingerprints-in-the-optical-and-transport-properties-of-quantum-dots/quantum-mechanics-of-semiconductor-quantum-dots-and-rings

INTECH
open science | open minds

**InTech Europe**
University Campus STeP Ri
Slavka Krautzeka 83/A
51000 Rijeka, Croatia
Phone: +385 (51) 770 447
Fax: +385 (51) 686 166
www.intechopen.com

**InTech China**
Unit 405, Office Block, Hotel Equatorial Shanghai
No.65, Yan An Road (West), Shanghai, 200040, China
中国上海市延安西路65号上海国际贵都大饭店办公楼405单元
Phone: +86-21-62489820
Fax: +86-21-62489821

IntechOpen